1 2 9 0

UNIVERSIDADE D
COIMBRA

João Pedro Sousa Mota

ACOUSTIC ASSESSMENT OF A NOVEL VISOR CONCEPT WITH AERODYNAMIC SEALING FOR MEDICAL PROTECTION

VOLUME 1

Dissertação no âmbito do Mestrado em Engenharia Mecânica, na especialidade de Energia e Ambiente, orientada pelo Professor Doutor Adélio Manuel Rodrigues Gaspar e pelo Professor Doutor Nuno Cláudio Ferreira Rosa, e apresentada ao Departamento de Engenharia Mecânica da Faculdade de Ciências e Tecnologia da Universidade de Coimbra.

Julho de 2023

1 2 9 0

FACULDADE DE CIÊNCIAS E TECNOLOGIA
UNIVERSIDADE D COIMBRA

Acoustic assessment of a novel visor concept with aerodynamic sealing for medical protection

A dissertation submitted in partial fulfilment of the requirements for the degree of Master in Mechanical Engineering in the speciality of Energy and Environment

Avaliação acústica de um novo conceito de viseira com vedação aerodinâmica para proteção médica

Author

João Pedro Sousa Mota

Advisors

Adélio Manuel Rodrigues Gaspar

Nuno Cláudio Ferreira Rosa

Committee

Chair	**Professor Doutor José Joaquim da Costa** **Professor Associado da Universidade de Coimbra**
Member	**Professor Doutor Manuel Carlos Gameiro da Silva** **Professor Catedrático da Universidade de Coimbra**
Advisor	**Professor Doutor Nuno Cláudio Ferreira Rosa** **Professor Auxiliar Convidado da Universidade de Coimbra**

Coimbra, July, 2023

“Absence of evidence is not evidence of absence”

Carl Sagan

Aos meus pais e irmãos.

ACKNOWLEDGEMENTS

I am deeply grateful to Professor Adélio Gaspar and Professor Nuno Rosa for their exceptional guidance and unwavering support during my dissertation. Their expertise and mentorship have played a pivotal role in shaping the direction and excellence of my research. I would also like to extend my appreciation to Professor Manuel Gameiro for his valuable contribution, providing the necessary software for this study and offering valuable scientific advice. Lastly, I express my gratitude to Professor Mário Mateus for his assistance in the calibration procedure and invaluable scientific guidance.

I am also deeply thankful to my friends for their unwavering support and encouragement during my academic journey. Their presence, engaging discussions and friendship have enriched my experience and made the challenges more manageable.

I would like to extend a special thank you to my girlfriend for her constant love, understanding, and support. Her unwavering presence has been a source of motivation and comfort throughout this endeavour.

Last but certainly not least, I want to express my sincere gratitude to my loving family. Your belief in me and your constant encouragement have been the pillars of my success. I am truly blessed to have you by my side.

This work was funded by FEDER - European Regional Development Funds through the operational program Centro 2020 of Portugal 2020 according to Support System for Scientific and Technological Research (SAICT) in the framework of the project “VV4MC – A new type of ventilated visor for medical care” (CENTRO-01-0145-FEDER-181248).

Abstract

In response to the COVID-19 pandemic, Personal Protective Equipment (PPE) such as masks and visors, have become essential for medical professionals to ensure their own safety and the safety of their patients. Several studies have demonstrated the potential of other viruses to be transmitted via the air. Additionally, the need for PPE remains significant, considering potential future pandemics. Conventional face masks can sometimes hinder communication and comfort. On the other hand, visors are comparatively more comfortable and provide protection against contamination through the eyes. To address these challenges, a consortium composed of SETsa (Sociedade de Engenharia e Transformação S.A.), ADAI (Association for the Development of Industrial Aerodynamics), and FMUC (Faculty of Medicine of the University of Coimbra) developed the MASK4MC, a visor with aerodynamic sealing that combines protection efficiency and user comfort.

This study was conducted as part of the VV4MC project, aiming to optimize the existing design of MASK4MC. It focused on assessing and improving the acoustic performance of the PPE, as it inherently generated noise during operation. Various methods were employed, including measuring noise levels, conducting frequency analysis, evaluating the Articulation Index (AI) and Speech Intelligibility Index (SII), and assessing speech attenuation of the final PPE prototype using white noise.

The optimisations made from the initial to the final prototype resulted in a significant reduction of PPE noise levels. For air flowrates of 15 to 30 l/min, the noise levels decreased from 20 to 30 dBA, with a maximum of 45.2 dBA in the final solution. Speech intelligibility improved from poor to excellent, with SII values close to 1 across all air flowrates in the final solution. When comparing speech attenuation, the final solution showed slightly inferior performance compared to the surgical mask and FFP2 respirator, although the differences were not significant.

Keywords: Acoustic Assessment, Personal Protective Equipment, VV4MC, Speech Intelligibility, Medical Protection.

Resumo

Em resposta à pandemia de COVID-19, o Equipamento de Proteção Individual (EPI), como máscaras e viseiras, tornou-se essencial para os profissionais de saúde garantirem a sua segurança e a dos seus pacientes. Estudos têm indicado o potencial de transmissão de vírus por via aérea. A necessidade de EPIs continua a ser importante, considerando a proteção contra outro tipo de vírus e possíveis futuras pandemias. As máscaras faciais convencionais podem, por vezes, comprometer a comunicação e o conforto, enquanto as viseiras são mais confortáveis e proporcionam proteção contra o contágio através dos olhos. Para enfrentar esses desafios, um consórcio composto pela SETsa (Sociedade de Engenharia e Transformação S.A.), ADAI (Associação para o Desenvolvimento da Aerodinâmica Industrial) e FMUC (Faculdade de Medicina da Universidade de Coimbra), desenvolveu a MASK4MC, uma viseira com vedação aerodinâmica que combina eficiência de proteção e conforto para o utilizador,

Este estudo foi desenvolvido como parte do projeto VV4MC, com o objetivo de otimizar o *design* existente da MASK4MC. O foco foi avaliar e melhorar o desempenho acústico do EPI, durante a sua utilização. Foram utilizados diversos métodos, incluindo a medição dos níveis de ruído, análise de frequência, avaliação do Índice de Articulação (AI) e do Índice de Inteligibilidade da Fala (SII). Também foi avaliada a atenuação da fala para o protótipo final do EPI, utilizando ruído branco.

Finalmente, as otimizações realizadas desde o protótipo inicial até ao protótipo final resultaram numa redução significativa nos níveis de ruído do EPI, de 20 a 30 dBA para caudais de ar de 15 a 30 l/min, com um máximo de 45.2 dBA, na solução final. A inteligibilidade de fala melhorou de fraca para excelente, com valores de SII próximos de 1 em todos os caudais de ar na solução final. Ao comparar a atenuação da fala, a solução final apresentou um desempenho ligeiramente inferior em relação à máscara cirúrgica e ao respirador FFP2, embora as diferenças não tenham sido significativas.

Palavras-chave: Avaliação Acústica, Equipamento de Proteção Individual, VV4MC, Inteligibilidade de Fala, Proteção Médica.

Contents

LIST OF FIGURES

LIST OF TABLES

LIST OF SIMBOLS AND ACRONYMS/ ABBREVIATIONS

List of Symbols

A_i – Band auditability function

B_i – Maximum of N_i' and V_i

b – Step-width designator

$bw_{\%}$ – Percentage bandwidth

C_i – Slope per one-third octave of the upward spread of the masking

D_i – Equivalent disturbance spectrum level

E_i' – Speech equivalent spectrum levels

F_i – Nominal midband frequency in each computation band

f_m – Nominal mid-frequencies

f_1 – Lower frequency limit

f_2 – Upper frequency limit

G – Octave ratio

I_i – Band importance function

K_i – Temporary variable for the auditability function calculation

$\bar{L}$ – Average sound pressure level

L_{eq} – Equivalent continuous sound pressure level

$L_{\mathrm{eq},PPE}$ – Equivalent continuous sound pressure level of the PPE

$L_{eq,room}$ – Equivalent continuous sound pressure level of the room

$L_{eq,tot}$ – Total equivalent continuous sound pressure level

$L_{p,\mathrm{eq}T}$ – Short-time equivalent continuous sound pressure level

L_{pt} – Total sound pressure level

MSL_i – Measured Sound Levels

N_i' – Noise equivalent spectrum levels

n – Number of measurements

p – Instantaneous sound pressure

p_0 – Reference sound pressure in the air

p_{rms} – Root-mean-square sound pressure

p_{τ} – Time-weighted sound pressure

t – Time

T – Total duration of the measurement

T_i' – Hearing threshold equivalent spectrum levels

TSL_i – Typical Speech Levels

U_i – Standard speech spectrum level at the normal vocal effort

V_i – Self-speech masking spectrum

X_i – Reference internal noise spectrum level

X_i' – Equivalent internal noise spectrum level

Z_i – Equivalent masking spectrum level

$\Delta(f)$ – Bandwidth of each frequency band

$\Delta_0 f$ – Reference bandwidth

Ø – Diameter

Acronyms/Abbreviations

ADAI – Association for the Development of Industrial Aerodynamics

ANSI/ASA – American National Standards Institute/ Acoustical Society of America

AI – Articulation Index

CFD – Computacional Fluid Dynamics

FMUC – Faculty of Medicine of the University of Coimbra

IEC – International Electrotechnical Commission

ISO – International Organization for Standardization

MASK4MC – Mask for Medical Care

PPE – Personal Protective Equipment

RMS – Reactive Muffler Splitter

SETsa – Sociedade de Engenharia e Transformação S.A

SII – Speech Intelligibility Index

VV4MC – Ventilated Visor for Medical Care

Ys – Y streamlined

Greek Symbols

τ – Time constant

1. INTRODUCTION

In this introductory chapter the research study is presented, by providing essential context and background information. It aims to present the research question and objectives and outline the overall structure of the work.

1.1. Context

In the wake of the COVID-19 pandemic, Personal Protective Equipment (PPE) such as masks and visors have become essential for medical professionals to protect themselves and their patients. Several studies have demonstrated the potential of other viruses to be transmitted via the air [1]–[4]. Additionally, the possibility of future pandemics remains a concern [5], [6], highlighting the importance of PPE. However, the use of conventional face masks can sometimes compromise communication and comfort [7], [8]. On the other hand, visors enhance the comfort aspect, and provide protection against contamination through the eyes [9]–[12].

As a result, there has been a growing interest in developing innovative PPE that can provide both protection and enhanced comfort. To address this issue, various approaches have been explored, with some making use of the air curtain technology alone [13]–[16], whilst others attempt to combine it with a visor [17], [18]. The air curtain refers to a system that uses a continuous air flow to create a barrier between two different environments.

Implementing an air curtain requires the use of an air supply system, which inherently generates noise. Noise is typically defined as an unwanted or disturbing sound [19]–[22], and can be classified into two main types: environmental noise and occupational noise, which occur in various settings such as communities, residential areas, domestic spaces, and workplaces [21], [24]–[26]. Noise is a pervasive risk factor, present in everyday activities, affecting a large number of individuals. It is estimated that 1.5 billion people are currently living with hearing loss, and this number is expected to increase in the coming years [26]. Besides hearing impairment, noise can have other effects on human health, such as hypertension [24], annoyance [27]–[29], decrease in mental performance [25],[30], stress,

fatigue, tinnitus. Therefore, it is crucial to assess and study solutions to reduce the noise levels of this PPE.

Within the context of this study, a consortium composed of SETsa (Sociedade de Engenharia e Transformação S.A.), ADAI (Association for the Development of Industrial Aerodynamics), and FMUC (Faculty of Medicine of the University of Coimbra) collaborated to develop the MASK4MC, a visor with aerodynamic sealing that combines protection efficiency and user comfort.

From the literature review it should be underlined that none of the previous studies have investigated the noise levels produced by this type of PPE. Hence, the main objective of the present work is to address this research gap by assessing and optimising the acoustic performance of the PPE, which is an integrated part of the VV4MC project.

1.2. Description of the Personal Protective Equipment (PPE)

The PPE under investigation, known as MASK4MC (Mask for Medical Care), was developed to provide healthcare workers with a comfortable fit while allowing them to use a surgical mask and a FFP2 respirator. It was registered in Portugal as a “utility model” [18]. The initial MASK4MC prototype, depicted in Figure 1.1, consists of a face shield (A) which confines an air curtain supplied by a plenum (B). The face shield serves as a protective shield against larger droplets, preventing them from impacting the user's face. Additionally, the air curtain seals the PPE, acting as a barrier to prevent small particles from entering around the face shield and potentially being inhaled by the user. A support system (C and D) is in place to ensure a proper fit and adjustment to the wearer's head, while also connecting the face shield and the plenum together using four screws (J). An air compressor system supplies air through a tube (E) to maintain the air curtain. The air is then split into two tubes in the T-shaped splitter (F) and fed into two inlets (G), before entering the plenum. The air flow enters the plenum chambers (K) and there, it is controlled by two types of geometries: 1) the two polymeric perforated filters (I), with 1 mm diameter holes, spaced 2 mm apart from each other; 2) and a wall (M) upstream of the jet slots (H), which helps increasing the uniformity of the air flow near the air vents. These strategies aim to achieve a consistent velocity of air

flow through slots 2, 3, and 4, while slot L maintains a higher velocity and specific angle to close up the visor lateral sides [31].

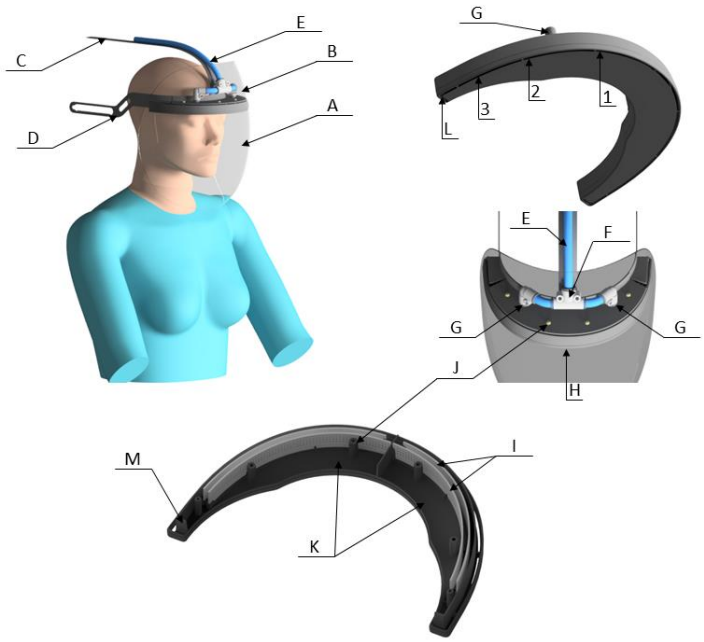

Figure 1.1: MASK4MC illustration.

The results obtained from the CFD simulation [31] demonstrate the distribution and control of airflow achieved through the implemented strategies (Figure 1.3), leading to the desired average velocities observed at the jet slots, as seen in the velocity contours in Figure 1.2.

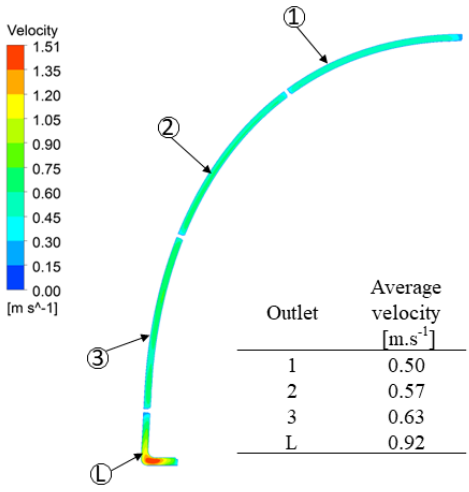

Outlet	Average velocity [m.s^{-1}]
1	0.50
2	0.57
3	0.63
L	0.92

Figure 1.2: Velocity contours. Adapted from [31].

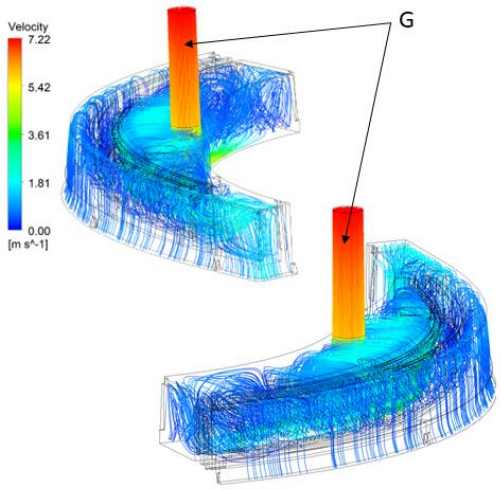

Figure 1.3: Air flow streamlines. Adapted from [31].

Following the jet slots, the air flow continues and forms the air curtain, effectively sealing the PPE. This is visually illustrated by the flow streamlines depicted in Figure 1.4.

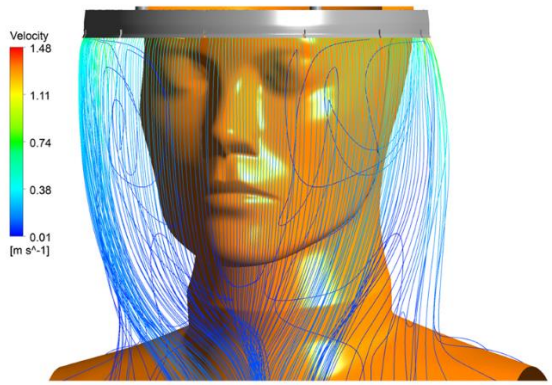

Figure 1.4: Air curtain streamlines. Adapted from [31].

1.3. Objectives and Research Framework

Following the completion of the MASK4MC project, a new initiative called VV4MC (Ventilated Visor for Medical Care) has been initiated. The objective of the VV4MC project is to enhance and validate the PPE for eventual deployment within the National Health Service, ensuring its availability for medical professionals.

In the previous studies the need to assess and mitigate the noise levels produced by this system was discussed. Therefore, the main objective of the present work is to address this research gap by assessing and optimising the acoustic performance of the previously described PPE, which is an integral part of the VV4MC project.

The study will begin with an initial iteration of the PPE [18] which will be tested at different air flowrates. Then, modifications will be implemented and tested as part of the optimisation effort. The evaluation of the acoustic performance will involve comprehensive analysis, including measurement of noise levels, frequency analysis, and Articulation Index (AI) and Speech Intelligibility Index (SII) evaluation. Additionally, a comparative study will be conducted to assess the effect of wearing the PPE from this study on speech compared to commonly used PPEs, such as surgical masks and FFP2 respirators. In the upcoming chapters, key concepts, and relevant terminology to the study will be described. This will be followed by a detailed explanation of the experimental setup, procedures and all the modifications tested. Lastly, the results will be presented and thoroughly discussed, leading to meaningful conclusions based on the obtained findings.

2. MATERIALS AND METHODS

2.1. Concepts and Terminology

This section aims to provide a comprehensive overview of the key concepts and terminology that will be used throughout the study. In addition, it will introduce the type of analysis that will be conducted, thereby enhancing the understanding of the study's outcomes.

2.1.1 Sound and Sound Pressure Level

Sound is a form of mechanical disturbance that travels through a specific medium, such as air, at a characteristic speed. The propagation of sound is essentially a wave phenomenon, relying on the mechanical properties of the medium for its propagation. In other words, sound requires a physically elastic medium through which it can travel and be perceived [32]. As sound waves pass through a specific location, they induce particle oscillation, resulting in alternating compression and rarefaction of the medium. These oscillations create pressure fluctuations within the stationary environment, known as sound pressure [19]. Sound pressure, is defined in the ISO 80000-8:2020 [33] as the difference between instantaneous total pressure and the static pressure, expressed in the SI-unit of pascal (Pa). A way of quantifying these pressure fluctuations is to square the values of the sound pressure over a period of time. The root-mean-square sound pressure (p_{rms}) is defined as [32]:

$$p_{rms} = \sqrt{(p)^2} = \sqrt{\frac{\int_0^\tau p^2 dt}{\int_0^\tau dt}}\ [Pa]\,, \tag{2.1}$$

where τ is the time interval of the measurement and the p is the instantaneous sound pressure. However, the human ear is capable of perceiving a wide range of sound pressures [19], [20],discarding the possibility to accurately represent the full range accurately on a linear scale. As such, a logarithmic scale is employed to compress the range of values into a more manageable arrangement [34]. The sound pressure level (L_p), measured in decibel

(dB), is used to express the sound pressure. Sound pressure level exhibits a logarithmic dependence on the sound pressure as follows [32], [35], [36]:

$$L_p = 10\,log_{10}\left(\frac{p_{rms}}{p_0}\right)^2\ [dB]. \tag{2.2}$$

p_0 is the reference value for sound pressure in the air. This value is equal to 20 µPa, a standardised quantity representing the root-mean-square pressure at a frequency of 1000 Hertz (Hz). It is considered the threshold of human hearing and corresponds to a sound pressure level of 0 dB [19], [21], [36]–[38]. Equation (2.2) can be rewritten in order to calculate the sound pressure, as shown below:

$$p_{rms} = p_0 10^{\frac{L_p}{20}}\ [Pa]. \tag{2.3}$$

Using the equation above, a sound pressure level (L_p) of 140 dB corresponds to a sound pressure of 200 Pa, which is ten million times greater than the reference value of 20 µPa. This significant difference in magnitude between the two values justifies the use of a logarithmic scale instead of a linear one allowing for an effective representation of the wide range of sound pressure levels commonly observed in practical applications.

2.1.2. Subtraction, Addition and Averaging of Sound Pressure Levels

Since sound pressure levels are expressed in decibel (dB), their logarithmic nature requires a linear scale conversion prior to any mathematical operation. The addition of sound pressure levels can be done using the equation [32]:

$$L_{pt} = 10log_{10}\left(\sum_{i=1}^{n} 10^{\frac{L_{pi}}{10}}\right)\ [dB], \tag{2.4}$$

where, n represents the total number of measurements and i refers to the i-th measurement in the sequence. The resulting value (L_{pt}), represents the total sound pressure level, in decibel (dB). When averaging, the following equation can be used, as defined in [38]:

$$\bar{L} = 10log_{10}\left(\frac{\sum_{i=1}^{n} 10^{\frac{L_{pi}}{10}}}{n}\right)\ [dB]. \tag{2.5}$$

$\bar{L}$ is the average sound pressure level for *n* measurements. As for subtraction, this operation is useful when calculating the sound pressure level of a specific source. As previously mentioned, the study will aim to obtain noise levels generated by the PPE alone ($L_{\mathrm{eq},PPE}$). The following approach will be employed consistently throughout the research:

$$L_{\mathrm{eq},PPE} = 10log_{10}\left(10^{\frac{L_{eq,tot}}{10}} - 10^{\frac{L_{eq,room}}{10}}\right)\ [dB]. \tag{2.6}$$

Here, the $L_{eq,tot}$ is the equivalent continuous sound pressure level (see Equivalent Continuous Sound Pressure Level) of the room's ambient noise with the air supply on. The $L_{eq,room}$ refers to the room's ambient noise alone, i.e., the baseline measurement. The $L_{\mathrm{eq},PPE}$ is one of the key parameters in this study.

2.1.3. Time-Weighting

The time-weighting setting has a significant influence on how sound levels are measured and how they change over time. In accordance with the IEC 61672-1 [39], two time-weightings are recognised: "S" for Slow and "F" for Fast, with an associated time constant (τ) of 1 second and 0.125 seconds, respectively. The time-weighted sound pressure levels are calculated using equation (2.1) by replacing p with an exponentially time-weighted sound pressure (p_τ). The p_τ considers not only the current sound pressures but also those that have occurred in the past. The Fast time-weighting setting is more responsive to changes in sound levels compared to the Slow time-weighting setting due to its reduced emphasis on past sound pressures. Additionally, the time constant plays a crucial role in stabilising sound levels, indicating the time required to transition from one sound level to another. This can be demonstrated using the following expression [37]:

$$\frac{4.34}{\tau}. \tag{2.7}$$

For example, when transitioning from a steady 90 dB signal to a steady 70 dB signal with a Slow time constant ($\tau = 1$ second), the sound level will decrease at a rate of 4.34 dB per second, taking approximately 4.6 seconds to stabilise. However, with a Fast time constant (τ = 0.125 seconds), the same change will occur at a rate of 34.72 dB per second, stabilising in roughly 0.6 seconds, which is almost eight times faster. Therefore, when

measuring an unsteady signal and aiming for improved precision, the Fast setting is more suitable.

2.1.4. Frequency-Weighting

Human beings can perceive sound frequencies ranging from 20 to 20,000 Hz [19], [21], [41]. However, hearing sensitivity varies within this range, which is why frequency-weighting filters are used for measurements purposes. The IEC 61672-1:2013 [39], specifies three frequency weightings:

• A-Weighting: designed to approximate the frequency response of the human ear. Through a mathematical function, it attenuates low and high frequencies and amplifies the mid-frequencies [37], the most sensitive range of human hearing. It is the most widely used and, typically, exposure limits [41], [42] are based on this weighting.

• C-Weighting: considered to have a similar response to the human ear for loud sounds, giving more emphasis on the lower frequencies than the previous one. It is "flat" from 32 to 8000 Hz but attenuates below and above this range [37]. It is commonly used to make peak sound measurements [43].

• Z-Weighting: has a weighting characteristic of 0 dB from 10 to 20,000 Hz, i.e., this filter does not attenuate or amplify the signal [43].

Since the use of frequency-weighting will alter the values of a sound level measurement, it is necessary to specify which one was used. This is done by adding the corresponding weighting symbol in the measured parameter or its unit, e.g., L_{pA} and dBA respectively. The analytical expressions for each frequency-weighting can be found in IEC 61672-1:2013 [39].

2.1.5. Equivalent Continuous Sound Pressure Level

The purpose of the equivalent continuous sound pressure level (L_{eq}) is to obtain a more stable and accurate representation of the sound pressure level over the time, especially for fluctuating and intermittent sound sources. By averaging the sound pressure level over a

longer period of time, the effects of the short-term variations are reduced. In simple terms, this stable value has the same average energy and duration as its unsteady counterpart [36], [38]. The equivalent continuous sound pressure level (L_{eq}), can be calculated using the equation defined in the ISO 3740:2019 [35]:

$$L_{\mathrm{eq}} = 10log_{10}\left[\frac{\frac{1}{T}\int_{t_1}^{t_2} p^2(t)dt}{p_0^2}\right] [dB], \tag{2.8}$$

where, T is the total duration of the measurement, starting at t_1 and ending at t_2. To streamline the digital processing [32], the calculation of the equivalent continuous sound pressure level (L_{eq}) can be simplified by using a short time interval *T*, such as 0.125 seconds or 1 second, which are commonly used in Fast and Slow time-weightings [37]. In this study, a timestep of 0.125 seconds will be employed. The L_{eq} is determined by an equivalent summation of the measured $L_{p,\mathrm{eq}T}$ in each timestep, as follows:

$$L_{\mathrm{eq}} = 10log_{10}\left(\frac{1}{n}\sum_{i=1}^{n} 10^{\frac{L_{p,\mathrm{eq}T}(i)}{10}}\right) [dB], \tag{2.9}$$

where *n* is the total number of short-time equivalent continuous sound pressure levels ($L_{p,\mathrm{eq}T}$) over the measurement duration. The L_{eq} is a key parameter when assessing sound levels as it provides an accurate representation of the sound levels over the measurement period. In this study, A-weighted and Fast time-weighted L_{eq} values will be used to measure noise levels. This parameter is commonly used in occupational noise assessments, emphasising its importance for the present work.

2.1.6. Frequency Analysis

Frequency analysis is an essential tool that complements sound level measurements by providing critical information about the frequency content of a sound signal. By decomposing the sound signal into its individual frequency components [44], referred to as frequency bands, it enables a more comprehensive understanding of the sound spectrum and the identification of dominant frequencies. This is particularly important for evaluating the effectiveness of noise mitigation strategies, especially in reducing specific frequency band levels.

Due to the wide frequency range and the use of a logarithmic scale, a common practical approach in engineering is to use filters tuned to different frequencies [45]. This allows the

measurement of the sound pressure level in each frequency band, showcasing specific frequency ranges that require mitigation measures. This approach is widely used in occupational and environmental noise assessment [24], [25], [30], [44] as well as in the design of noise control measures for machinery and equipment [46]. In this study, frequency analysis will be conducted using one-third (1/3) octave bands.

An octave band is a frequency band where the ratio between the upper frequency limit (f_2) and lower frequency limit (f_1) is 2. This also applies for the mid-frequency of two consecutive bands. This ratio is defined in the IEC 61260-2:2016 [47] as the octave ratio (G), and for a base-ten system, it is defined as:

$$G = 10^{\left(\frac{3}{10}\right)\left(\frac{1}{b}\right)}, \tag{2.10}$$

where b is the step-width designator. For octave bands, the value for b is 1, so the octave ratio, as mentioned above, is approximately 2. The range between the lower and upper limit is known as the bandwidth. While these values can be calculated, standardised values known as nominal mid-frequencies (f_m), are used instead. All the nominal mid-frequencies have been fixed around a reference frequency of 1,000 Hz, which is the middle frequency in the range of audible frequencies due to the logarithmic nature of the scale. In this frequency, regardless of the weighting and filter used, there is no attenuation or amplification of the sound signal. The bandwidth is the difference between f_2 and f_1. If an octave band is equally divided into three separate frequency bands, a one-third (1/3) octave band is created. In this case, b takes a value of 3 and the octave ratio (G) is approximately 21/3.

The octave band filters are constant percentage bandwidth filters. For example, for a one-third octave frequency band, where the nominal mid-frequency is 1000 Hz, the lower frequency limit will be 891 Hz and the upper frequency limit 1122 Hz. The percentage bandwidth ($bw_{\%}$) of an octave band filter, can be calculated with the equation bellow [19]:

$$bw_{\%} \equiv \frac{f_2 - f_1}{f_m} \times 100. \tag{2.11}$$

For all one-third octave bands, the bandwidth percentage is around 23%, i.e., the bandwidth is 23% of the mid-frequency value. This means that, has the mid-frequency values increase, the bandwidth also increases proportionally. This is crucial since the frequency scale used for analysis is logarithmic, and constant percentage bandwidth ensures an equally

spaced representation of each frequency band on the logarithmic scale. This makes it easier to compare and analyse frequency components of a sound signal.

2.1.7. Articulation Index

Noise is commonly described as unwanted sound that can have numerous adverse effects on human health. One particular effect is the speech masking, where the presence of excessive noise impairs the audibility of speech [32]. The Articulation Index (AI) is a metric that assesses how well speech can be understood in the presence of background noise. It considers the clarity of different speech sounds and the influence of noise on their perception. Speech intelligibility depends on the sound pressure level and frequency components of the noise, so an idealised speech spectrum [48] measured at one meter from the lips was created. This spectrum covers speech frequencies between 200 Hz and 6100 Hz, with speech levels ranging from 55 dB to 70 dB (unweighted)[32].

The calculation of AI was first presented in the ANSI/ASA S3.5-1969. It can be done using the noise levels and the typical speech levels (TSL_i) at 1 meter for various frequency bands. Different frequency bands have different contributions, called weighting factors (w_i). Also, a peak factor in speech is considered by incrementing 12 dB to the typical speech levels at every frequency band [32]. Then the incremented values are subtracted by the measured sound levels (MSL_i). This is the value that will be multiplied by the weighting factors at each frequency band. Finally, the sum of each weighted contributions for every computation band (i) is divided by 10,000, and the AI is obtained. It ranges from 0, for completely unintelligible speech, to 1, the best speech intelligibility conditions. The procedure described can be computed by using the following equation:

$$AI = \frac{\sum_i [(TSL_i - MSL_i) \times w_i]}{10{,}000} \ [-]. \tag{2.12}$$

The typical speech levels and the weighting factors in each one-third octave bands used for calculation, can be consulted in table below:

i	Centre Frequency (Hz)	*TSL* [dB]	w_i [-]
1	200	67	4
2	250	68	10
3	315	69	10
4	400	70	14
5	500	68	14
6	630	66	20
7	800	65	20
8	1000	64	24
9	1250	62	30
10	1600	60	37
12	2000	59	37
13	2500	57	34
14	3150	55	34
15	4000	53	24
16	5000	51	20

Table 2.1: Weighting Factors and Typical Speech Levels (+ 12 dB) for One-Third Octave Bands [32].

In medical procedures, error-free communication is crucial for success. Therefore, it is important to evaluate the *AI* value in order to ensure effective communication. It should be noted that there is no single acceptable *AI* value for communications, as stated by Karl D. Kryter [49]. Undoubtedly, higher values will always correspond to improved communication quality.

2.1.8. Speech Intelligibility Index

The Speech Intelligibility Index (*SII*) was introduced as a revision of the S3.5 standard in the ANSI/ASA 3.5-1997 [50]. It builds upon the Articulation Index (*AI*) by incorporating a broader range of input variables. This expanded approach enables the *SII* to provide a more precise assessment of speech intelligibility compared to the *AI* [51]. The calculation procedure of the *SII* is described in the ANSI/ASA S3.5-1997 (R2020) [52]. In the present work, the one-third octave band method is used.

The calculation begins with the specification of equivalent spectrum levels at one-third octave band centre frequencies for speech (E_i'), noise (N_i') and hearing threshold (T_i'). In this case, a hearing threshold for a normal listener of 0 dB HL (Hearing Loss) in all frequency bands [20], and a standard speech spectrum level for a normal vocal effort were considered. The parameter's values for the SII calculation are listed in Table 2.2. The subindex i, refers to the computation band. The measured one-third octave band sound levels had to be converted to spectrum levels using the following equation:

$$N_i' = MSL_i - 10log_{10}\left[\frac{\Delta(f)}{\Delta_0 f}\right] \ [dB]. \tag{2.13}$$

The MSL_i are the measured sound levels in each one-third octave band, $\Delta(f)$ is the bandwidth of each frequency band and $\Delta_0 f$, the reference bandwidth of 1 Hz. Subsequently, the equivalent masking spectrum level (Z_i) is calculated. Initially, for each calculation band, the self-speech masking spectrum (V_i) is determined with the equation below:

$$V_i = E_i' - 24 \ [dB]. \tag{2.14}$$

Then, the slope per one-third octave of the upward spread of the masking (C_i):

$$C_i = -80 + 0.6[B_i + 10log_{10}F_i - 6.353] \ [dB/octave]. \tag{2.15}$$

Here, B_i is the maximum value between N_i' and V_i, and F_i the nominal midband frequency in each computation band (Table 2.2). Finally, the equivalent masking spectrum level is obtained as follows:

$$\begin{cases} Z_1 = B_1 \\ Z_i = 10log_{10}\left\{10^{0.1\times N_i'} + \sum_k^{i-1} 10^{0.1\times\left[B_k + 3.32\times C_k\times log_{10}(0.89\times\frac{F_i}{F_k})\right]}\right\} \end{cases} [dB]. \tag{2.16}$$

The summation index (k) runs from $i = 1$ to $i - 1 = 17$. To determine the band auditability function (A_i), first, the equivalent internal noise spectrum level (X_i') is determined:

$$X_i' = X_i + T_i' \ [dB]. \tag{2.17}$$

X_i is the reference internal noise spectrum level for each computation band, listed in Table 2.2. Next, the equivalent disturbance spectrum level (D_i) is obtained, which is equal to the maximum between Z_i and X_i'. The level distortion factor (L_i) is then calculated:

$$L_i = 1 - \frac{(E_i' - U_i - 10)}{160} \ [dB]. \tag{2.18}$$

where U_i is the standard speech spectrum level at the normal vocal effort, which, in this case, is equal to E_i' and can also be found in Table 2.2. Finally, a temporary variable (K_i) needs to be determined:

$$K_i = \frac{(E_i' - D_i + 15)}{30} \ [-]. \tag{2.19}$$

K_i constrained to be between 0 and 1, inclusive. If its calculated value exceeds 1, it is set to 1, and if its value is negative, it is set to 0. Now the band auditability function can be computed:

$$A_i = L_i K_i \ [-]. \tag{2.20}$$

The A_i is also constrained between 0 and 1. At last, the speech intelligibility index (SII) can be determined:

$$SII = \sum_{i=1}^{n} I_i \, A_i \ [-]. \tag{2.21}$$

Here, the I_i is the band importance function in each computation band, available in Table 2.2, and the SII is also limited between 0 and 1.

i	***F*$_i$ [Hz]**	***E*'$_i$ = *U*'$_i$ [dB]**	***T*'$_i$ [dB HL]**	***X*$_i$ [dB]**	***I*$_i$ [-]**
1	160	32.41	0	0.6	0.00830
2	200	34.48	0	-1.7	0.00950
3	250	34.75	0	-3.9	0.0150
4	315	33.98	0	-6.1	0.0289
5	400	34.59	0	-8.2	0.0440
6	500	34.27	0	-9.7	0.0587
7	630	32.06	0	-10.8	0.0653
8	800	28.30	0	-11.9	0.0711
9	1000	25.01	0	-12.5	0.0818
10	1250	23.00	0	-13.5	0.0844
11	1600	20.15	0	-15.4	0.0882
12	2000	17.32	0	-17.7	0.0898
13	2500	13.18	0	-21.2	0.0868
14	3150	11.55	0	-24.2	0.0844
15	4000	9.330	0	-25.9	0.0771
16	5000	5.310	0	-23.6	0.0527
17	6300	2.590	0	-15.8	0.0364
18	8000	1.130	0	-7.1	0.0185

Table 2.2: Values needed for the ***SII*** calculation procedure. Adapted from [52].

The procedure highlights the greater complexity of the SII compared to the AI, as it considers a broader range of factors, resulting in a more accurate prediction of speech intelligibility. Therefore, in this study the SII was chosen as the preferred measure. However, the AI results will also be presented in Appendix A for reference. According to guidelines provided by ANSI/ASA S3.5-1997 (R2020) [52], a good communication system is characterised by an SII of 0.75 or higher, while a poor communication system is defined by SII values of 0.45 or lower.

2.2. Instrumentation and Experimental Setup

The experiments were conducted in a low-noise environment to minimise external noise interference. A manikin (Brüel & Kjær Sound Quality Head and Torso Simulator Type 4100) was positioned inside a tent to prevent direct transmission of noise from the air supply system to the manikin. This manikin is designed to replicate the acoustic properties of the human ear and includes a built-in condenser microphone and preamplifier assembly. The microphone (Brüel & Kjær 1/2'' Free-field Microphone Type 4190) converts sound waves into an electrical signal, which is then amplified and conditioned by a preamplifier (Brüel & Kjær Preamplifier Type 2669-L) to ensure it is suitable for further processing. The signal is then transmitted to a conditioning amplifier (Brüel & Kjær Nexus Conditioning Amplifier Type 2690), which further processes and conditions the signal. The output signal is then fed into an Audio Interface (Roland Quad-Capture USB 2.0 Audio Interface), which performs signal processing and converts the analogue signal to digital format so it can be recorded and processed by a computer, connected via USB.

Three applications developed in LabVIEW by M. C. Gameiro da Silva [53]–[55] are used to record and process the sound data. The first application records the sound pressure level (L_p) and short-time equivalent continuous sound pressure level ($L_{p,\mathrm{eq}T}$) throughout measurement duration. The second application is used to record the equivalent continuous sound pressure level (L_{eq}) broken down into one-third octave frequency bands. The third application records the Articulation Index (AI) over the measurement duration. The results of each test are saved in a *.txt* file for further analysis. Figure 2.1 shows an illustration of the experimental setup.

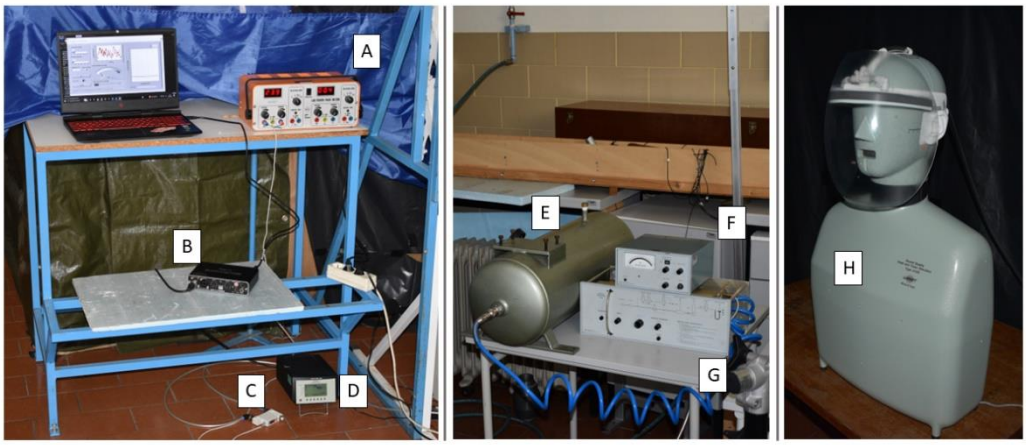

Figure 2.1: Experimental Setup illustration.

The sound measurement equipment was calibrated using a Brüel & Kjær Sound Calibrator Type 4231, which follows the guidelines outlined in the IEC 60942:2017 [56]. To calibrate the equipment, the microphone was inserted into the adaptor, and the preamplifier gain and microphone sensitivity were adjusted to achieve the target calibration value of 94 ± 0.2 dB. The calibration frequency was set at 1000 Hz, ensuring that the calibration value remains independent of the type of frequency weighting used. The calibration pressure for a 20 µPa reference pressure is 1 Pa. To verify the linearity, a level step of +20 dB was also included, producing a sound pressure level of 114 ± 0.2 dB. The results of the calibration procedure are presented in the figure below.

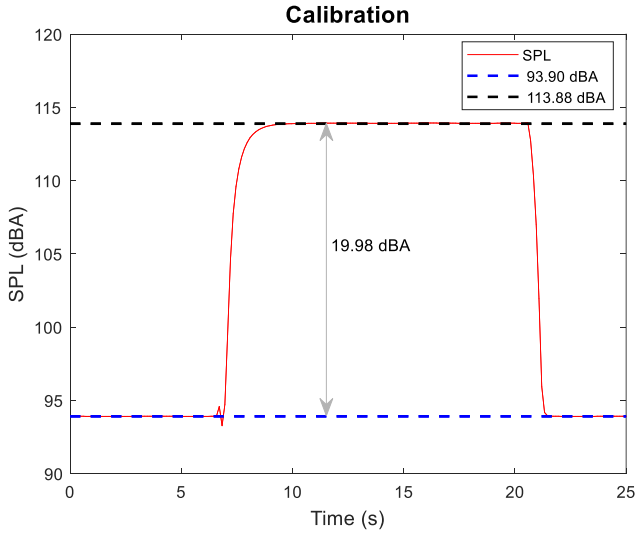

Figure 2.2: Calibration procedure.

The air supply system, placed outside the tent, consists of a compressor tank, a pressure converter (DISA Type 55 D46), a pressure control unit (DISA Type 55 D44), where the air flowrate is regulated, and compressed air piping (≈6 bar). Further downstream, a flow meter (SMC PFM711S-N02L-E-M), connected to a power supply (BEHA UNIWATT Lab Power-Pack NG 306), was used to check the air flowrate continuously.

The list of equipment and specifications are presented in the following table:

Equipment	**Purpose**	**Specifications**
Brüel & Kjær Sound Quality Head and Torso Simulator Type 4100	Simulates human ear acoustic properties for testing	-
Brüel & Kjær 1/2'' Free-field Microphone Type 4190	Measures sound pressure levels	Sensitivity: 50mV/Pa; Frequency response: 6.3Hz – 20 kHz; Dynamic range: 14.6 – 146 dB; Temperature range: –30 to +150 ºC (–22 to +302 ºF); Polarisation: 200V
Brüel & Kjær Preamplifier Type 2669-L	Amplifies microphone signals	Frequency response (re 1 kHz): 3 Hz to 200 kHz, ±0.5 dB; Attenuation: 0.35 dB (max); Phase linearity: ≤±3° from 20 Hz to 100 kHz
Brüel & Kjær Nexus Conditioning Amplifier Type 2690	Processes and conditions audio signals	Dynamic range: –30 to +10 dBV (peak); Resolution: 1 dB
Roland Quad-Capture USB 2.0 Audio Interface	Connects audio equipment to a computer	Input channels: 2; Output channels: 2; Bit depth: 24-bit; Sampling rate: 44.1kHz or 48kHz
Brüel & Kjær Sound Calibrator Type 4231	Microphone calibration	Sound Pressure Levels: 94.0 dB ±0.2 dB (Principal SPL) or 114.0 dB ±0.2 dB re 20 µPa; Frequency: 1 kHz ±0.1%

Table 2.3: List of equipment used in the experimental procedure.

2.3. Experimental Procedure

2.3.1. Measurements and Calculations

The initial step of the study involved conducting measurements to assess the impact of the PPE on ambient noise. This was achieved by measuring the L_{eq} values and one-third octave spectra for a duration of 30 seconds. The measurements were conducted under two conditions: without the PPE and with the manikin wearing the PPE.

To measure the sound levels, the data acquisition process initiates with the air supply system closed, in order to record the ambient noise level of the testing environment. Subsequently, the air supply was opened to the desired flowrate after approximately 45 seconds. To ensure stabilisation of the short-term equivalent continuous sound pressure level ($L_{p,\mathrm{eq}T}$), data acquisition continued for 105 seconds, thus yielding a total duration of 150 seconds for each test. The equivalent continuous pressure levels for both the ambient noise ($L_{eq,room}$) and total noise ($L_{eq,tot}$) were calculated using equation (2.9), with data ranging from 15 to 45 seconds and from 120 to 150 seconds respectively. The noise levels generated by the PPE were then determined using equation (2.6).

Similar procedures were followed for the tests conducted to determine the Articulation Index (AI), with data collected between 120 to 150 seconds and the average and standard deviation calculated accordingly. The calculations for the Speech Intelligibility Index (SII) were performed using an Excel spreadsheet. The frequency spectra levels were used as input data for the calculations.

To generate the frequency spectra for all configurations, tests were conducted with the air supply continuously on at a specific air flowrate for a duration of 30 seconds. This approach provided the total noise (L_{eq}) decomposed into the one-third octave frequency bands.

In this study, measurements were taken using A-weighting and Fast time-weighting settings.

2.3.2. Acoustic Assessments and Mitigation Strategies

The study had two main objectives: first, to assess the noise levels generated by the first iteration of the PPE (MASK4MC), and second, to investigate modifications aimed at reducing noise.

Several strategies were employed to mitigate noise. A first approach consisted of testing different tube diameters at different air flowrates. Subsequently, modifications were introduced, including the use of two types of splitters (T splitter and Y splitter), a muffler made of a porous medium housed in a connecting piece upstream of the splitter, and sideguards as physical barriers located on the lateral border ends of the PPE to provide better protection [57] and act as a sound barrier.

Tube thickness and insulation were also tested to assess their effectiveness in reducing noise propagation through the tubes. Additionally, a cone installed directly below the plenum air intake and a cushion placed on the plenum floor were tested to attenuate noise generated by the air's impact on the floor.

Lastly, two additional splitter strategies were tested: a Y splitter designed to cause less disturbance to the air flow (Ys) and a Reactive Muffler Splitter (RMS) that aimed to attenuate some of the noise coming from upstream.

In addition to their individual effectiveness in reducing noise levels, all of the strategies described were important in identifying noise sources. Through systematic testing of each strategy, sources of noise in the air supply system were isolated and identified, enabling the determination of the most effective approach to mitigate each specific source. The configurations considered are presented in the following table:

Configuration	PPE	Tube exterior-interior diameter [mm]	Air flowrates [l/min]	Splitter	Add-ons
1	MASK4MC	8-5.5	15-50	T	-
2	MASK4MC	8-5.5	15-50	Y	-
3	MASK4MC	6-4	15-50	Y	-
4	VV4MC	12-8	15-30	Y	-
5	VV4MC	12-8	15-30	Y	Muffler
6	VV4MC	12-8	15-30	Y	Sideguards
7	VV4MC	12-8	15-30	Y	Muffler + Sideguards
8	VV4MC	10-8	15-30	Y	-
9	VV4MC	10-8	15-30	Y	Muffler + Sideguards
10	VV4MC	10-8	15-30	Y	Cone
11	VV4MC	12-10	15-30	Y	-
12	VV4MC	12-10	15-30	Y	Muffler + Sideguards
13	VV4MC	12-10	15-30	Y	Cushion
14	VV4MC	12-10	15-30	Y	Cone
15	VV4MC	12-10	15-30	Y	Insulation
16	VV4MC	12-10	15-30	Ys	-
17	VV4MC	12-10	15-30	RMS	-
18	VV4MC	12-10	15-30	RMS	Muffler + Sideguards

Table 2.4: Configurations tested during the experimental procedure.

2.3.3. Assessing the Impact of Different PPE on Speech Levels

To investigate the potential impact of wearing PPE on speech levels, a comparative study was conducted involving different types of PPE. The study involved measuring the overall equivalent sound pressure level $L_{\mathrm{eq,tot}}$ and the one-third octave band spectra using a white noise signal emitted from a speaker (JBL Clip 4) positioned inside the manikin's head, right at its the mouth opening. The different PPE used, were placed on the manikin's head, covering the mouth opening. A microphone/preamplifier assembly (Brüel & Kjær Type 4190-L-002) was then mounted on a tripod at a distance of 2 meters from the manikin, as portrayed in Figure 2.3.

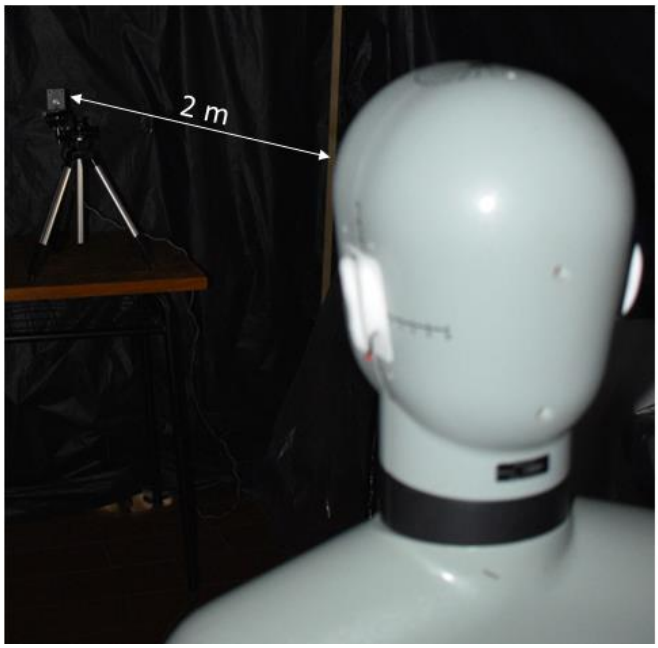

Figure 2.3: Manikin and microphone/preamplifier positioning.

Figure 2.4 illustrates the different scenarios in which the measurements were taken including without any mask or visor (1), with a surgical mask (2), with an FFP2 respirator (3), and with the PPE configuration used in this study at its most effective setting (4).

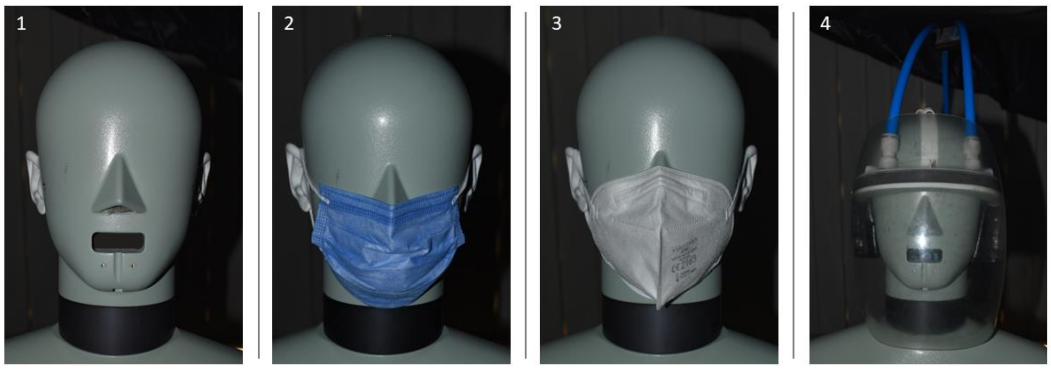

Figure 2.4: PPE placement on the manikin's head.

3. RESULTS AND DISCUSSION

3.1. PPE Impact on Ambient Noise

The effect of wearing the PPE on ambient noise levels measured at the manikin ear was evaluated, using $L_{p,\mathrm{eq}T}$ values and one-third octave spectra. The findings indicate that the impact of the PPE on ambient noise is negligible. Although the spectra in the mid-frequencies range were slightly affected (Figure 3.2), the $L_{p,\mathrm{eq}T}$ remained consistent at 35 dBA across both scenarios, as depicted in Figure 3.1.

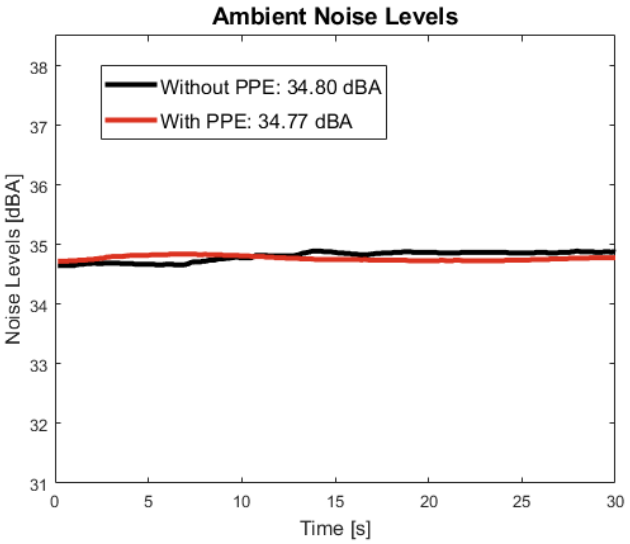

Figure 3.1: PPE impact on ambient noise levels

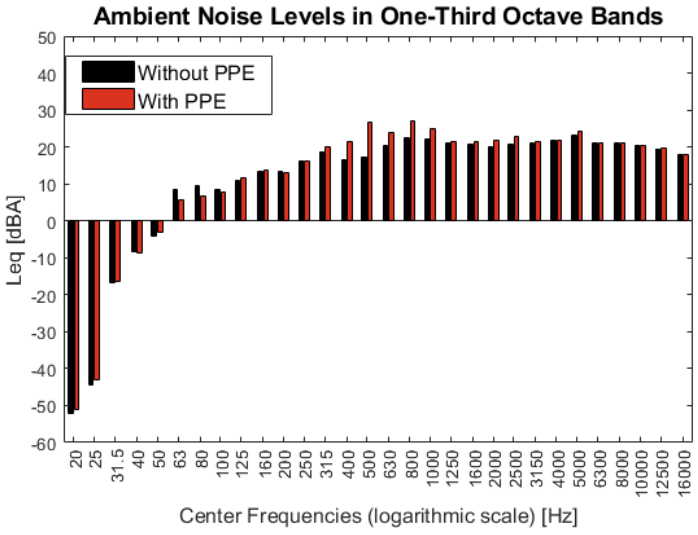

Figure 3.2: PPE impact on ambient noise spectra

3.2. Initial PPE Design and Y Splitter Modification

The initial PPE design (see Description of the Personal Protective Equipment (PPE)) was first tested, and later modified by changing the splitter from a T shape to a Y shape.

The purpose of this modification was to minimise air disturbance within the splitter and eliminate the curved connections that connect the tubes with the plenum inlets, as they introduce additional air flow disruptions (as shown in Figure 3.3).

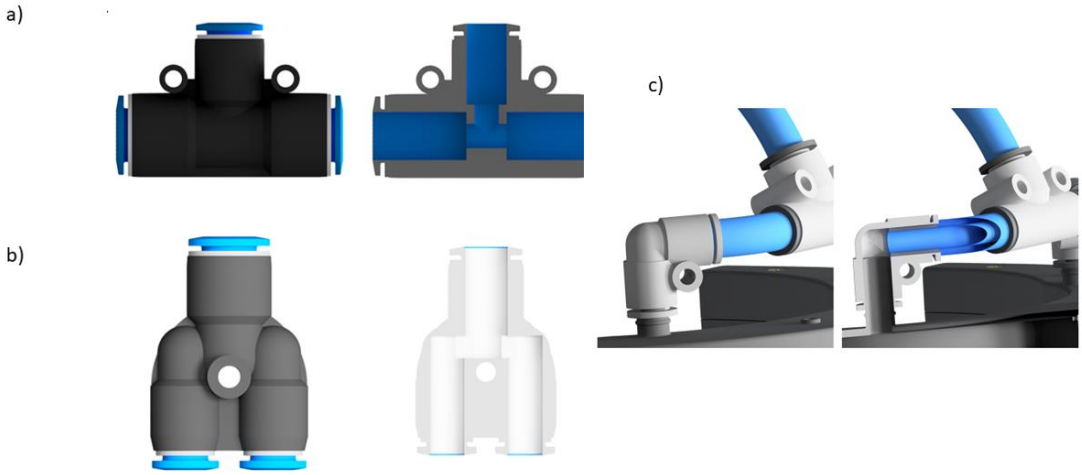

Figure 3.3: Splitter illustration: a) T Splitter; b) Y Splitter; c) Curved connection.

The results show a reduction in noise levels ($L_{\mathrm{eq},PPE}$) across all tested air flowrates and an increase in the Speech Intelligibility Index (SII) (Figure 3.4). As the flowrate increased, the noise reduction generally improved, with a maximum reduction of 6.7 dBA observed at 50 l/min. The results also indicated a correlation between air flowrate and noise levels, with higher air flowrates resulting in increased noise levels due to higher mean air velocities. This is supported by the one-third octave spectra, where the level in each frequency band increases as the flowrate increases (Figure 3.5).

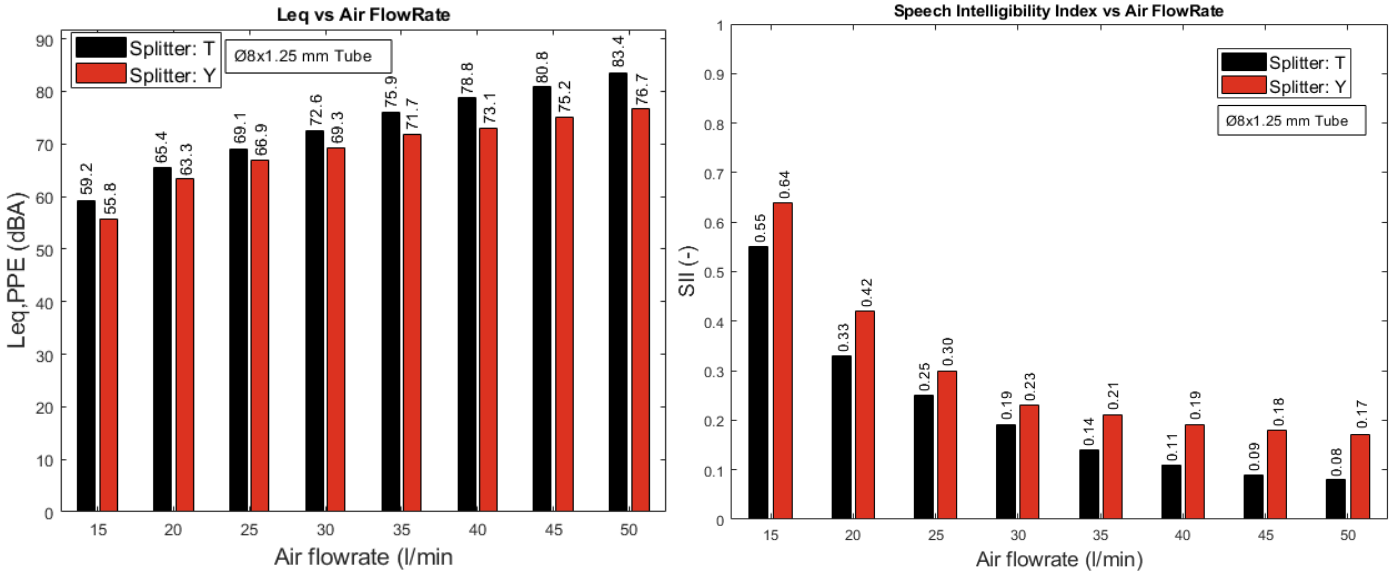

Figure 3.4: $L_{eq,PPE}$ and SII for different splitters and air flowrates.

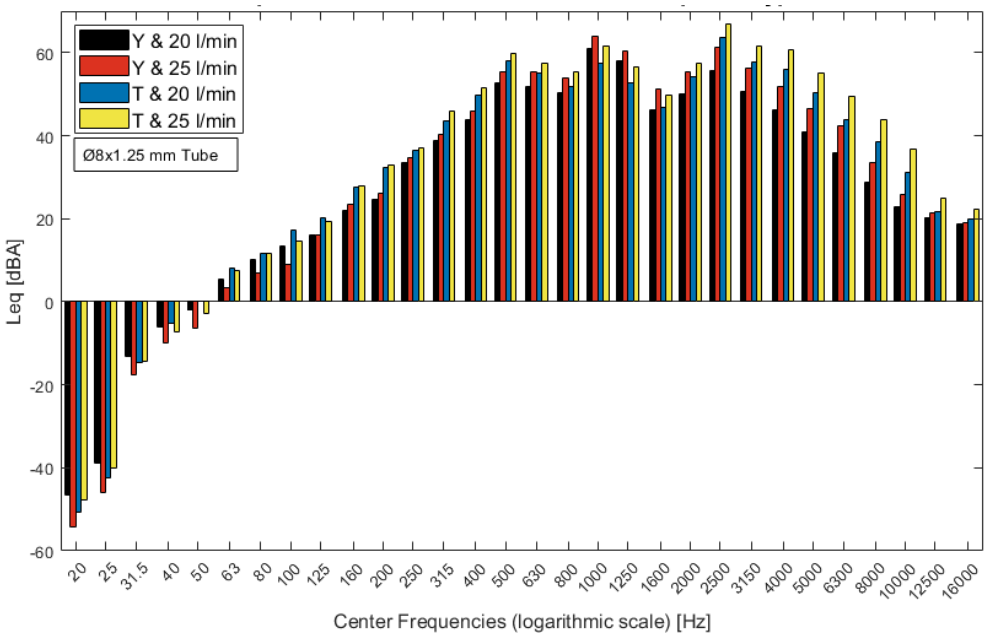

Figure 3.5: Spectra evolution with air flowrate and splitter type.

3.3. Airflow Rate and Tube Diameter

During the early stages of the experiment, it was observed that the noise levels were affected by the mean air velocity. To maintain a consistent air flowrate while minimising the impact of air velocity on noise levels, adjustments were made to the cross-sectional area of the air flow passage by varying the tube internal diameter. Figure 3.6 further supports this, as it was noted that increasing the tube internal diameter from 4 to 5.5 mm resulted in lower

noise levels. In this case, the maximum noise reduction of 18.4 dBA was observed at 15 l/min. However, increasing the air flowrate resulted in a decrease in the noise reduction. Also, for the Ø8x1.25 mm tube, significant improvements in the *SII* were observed at lower airflow rates.

Further analysis of the one-third octave band spectra revealed that increasing the tube diameter led a general attenuation across the spectrum, but more pronounced in the high frequencies (Figure 3.7).

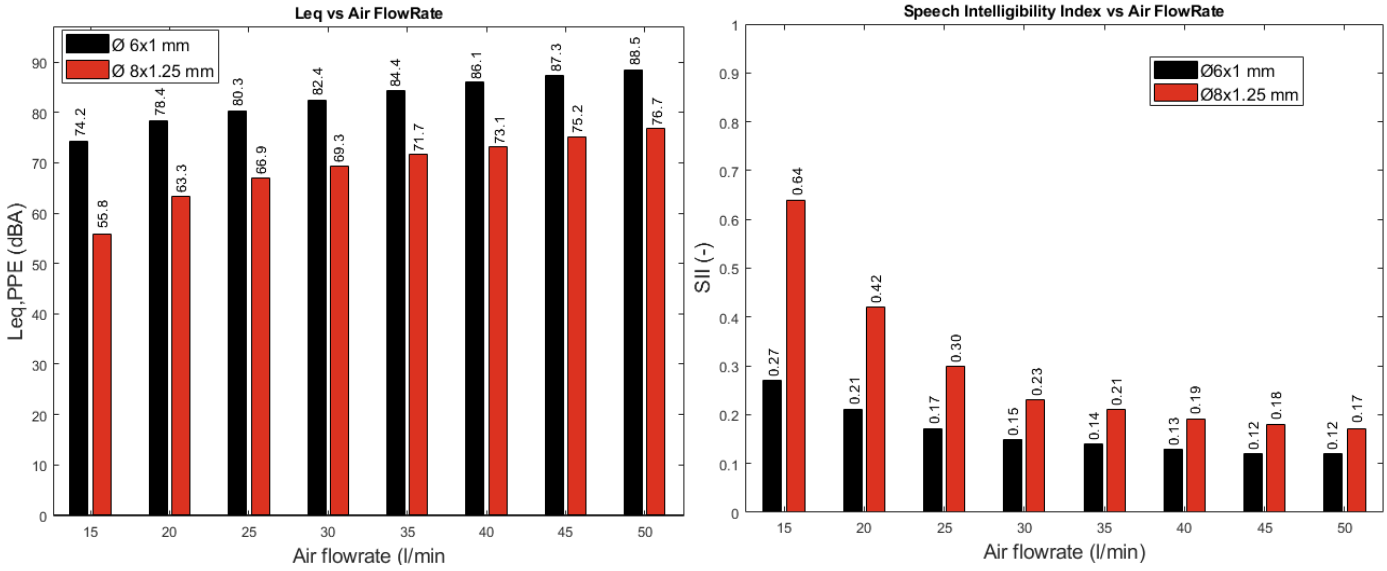

Figure 3.6: $L_{eq,PPE}$ and ***SII*** for different tube diameters and air flowrates.

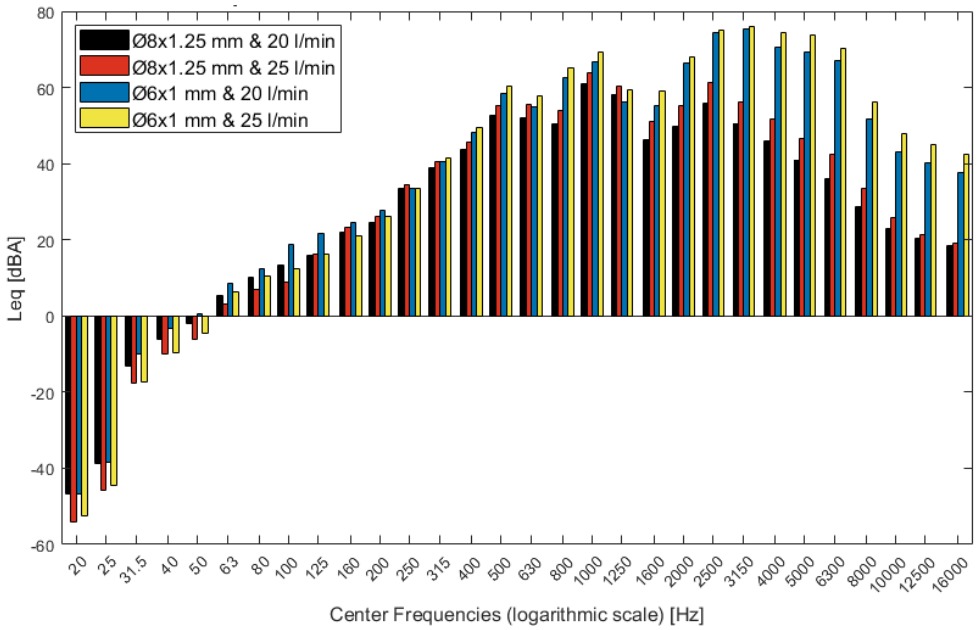

Figure 3.7: Spectra evolution with tube diameter and air flowrate

Then, the range of airflow rates being tested was reduced, as higher airflow rates generated more noise without a significant increase in protection efficiency, as demonstrated by Nuno Rosa *et. al* [31]. The experiment continued with larger tube internal diameters (8 and 10 mm) , which produced consistent results (Figure 3.8). The spectra showed a general decrease of noise levels across the entire range of frequency bands (Figure 3.9).

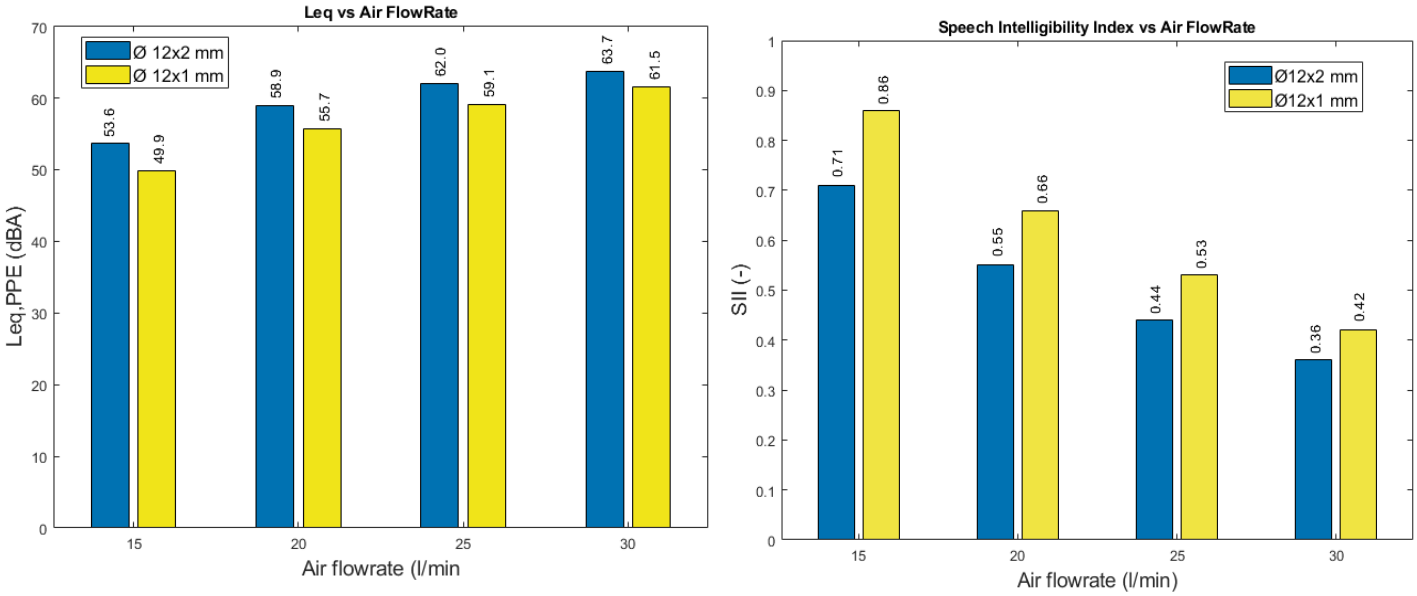

Figure 3.8: $L_{eq,PPE}$ and SII for different (larger) tube diameters and air flowrates (reduced).

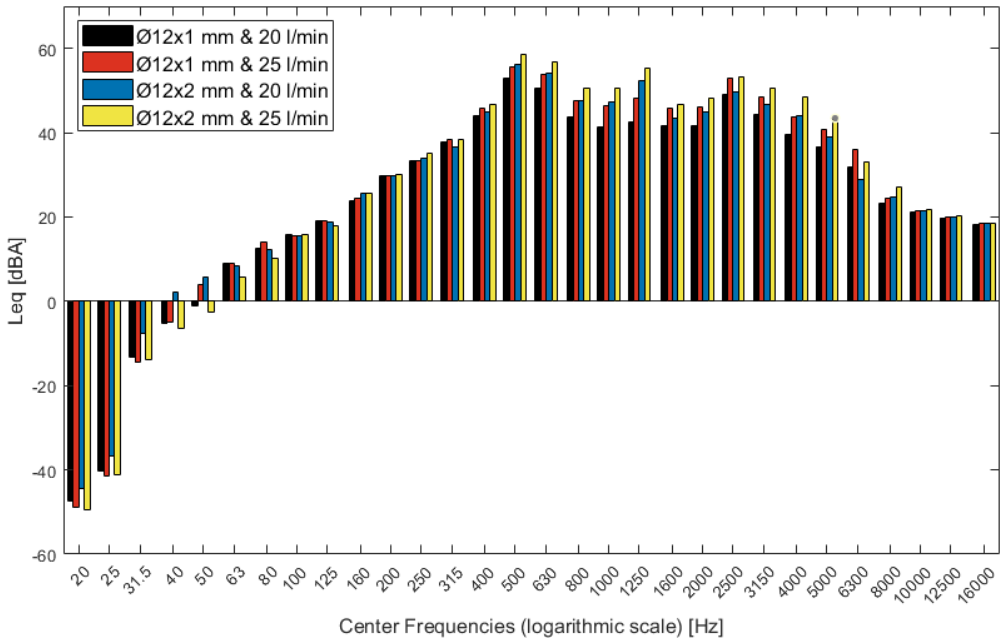

Figure 3.9: Spectra evolution with tube diameter (larger) and air flowrate (reduced).

3.4. Muffler & Sideguards

To further mitigate the noise produced by the PPE, additional components have been developed and incorporated into the setup. One of these components is the muffler, which consists of 3D printed parts designed to house a porous medium. Positioned approximately 1.5 meters upstream of the splitter, the muffler is intended to attenuate a portion of the noise coming from the air supply system. Inside, the porous medium intends to reduce turbulence in the air flow. Also, when sound waves interact with a porous material, they undergo three distinct transformations. Firstly, part of the sound waves is reflected towards the source. Secondly, part of the sound energy is absorbed by the porous material, leading to a conversion of the sound energy into mechanical energy and heat. Lastly, the remaining sound energy that is not absorbed passes through the porous material and continues to propagate [58], [59]. The technical drawing of the muffler assembly can be found in Appendix B.

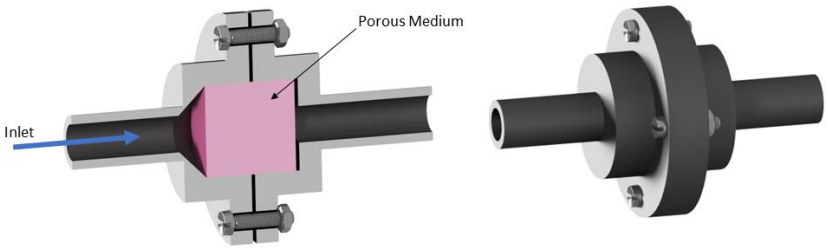

Figure 3.10: Illustration of the Muffler assembly.

The sideguards were implemented, as part of the efforts to enhance the PPE protection efficiency [57]. On top of that, as they are physical barriers to the noise coming from the jet slots, they have potential to reduce noise as well. Figure 3.11 displays the sideguards assembled in the PPE.

Figure 3.11: Sideguards assembly illustration

The study findings demonstrated the effective noise reduction capabilities of both the muffler and the sideguards when assessed individually. Notably, improvements were observed across all air flow rates. The muffler exhibited slightly superior performance in reducing noise levels compared to the sideguards, specifically at air flow rates of 15 and 30 l/min (Figure 3.12). However, when evaluating the *SII*, the sideguards surpassed the muffler. This was evident in the spectral analysis (Figure 3.13), where the sideguards' spectrum exhibited greater attenuation in the frequency bands spanning from 1000 Hz to 6300 Hz, resulting in a higher *SII*.

Combining the muffler and sideguards in the PPE configuration resulted in additional noise reduction. The *SII* achieved a value of 0.99 at an airflow rate of 15 l/min, with a minimum value of 0.68 at 30 l/min (Figure 3.12). This indicates that the combined modifications allowed for effective speech intelligibility. These findings further supported the integration of the muffler and sideguards into the final PPE prototype.

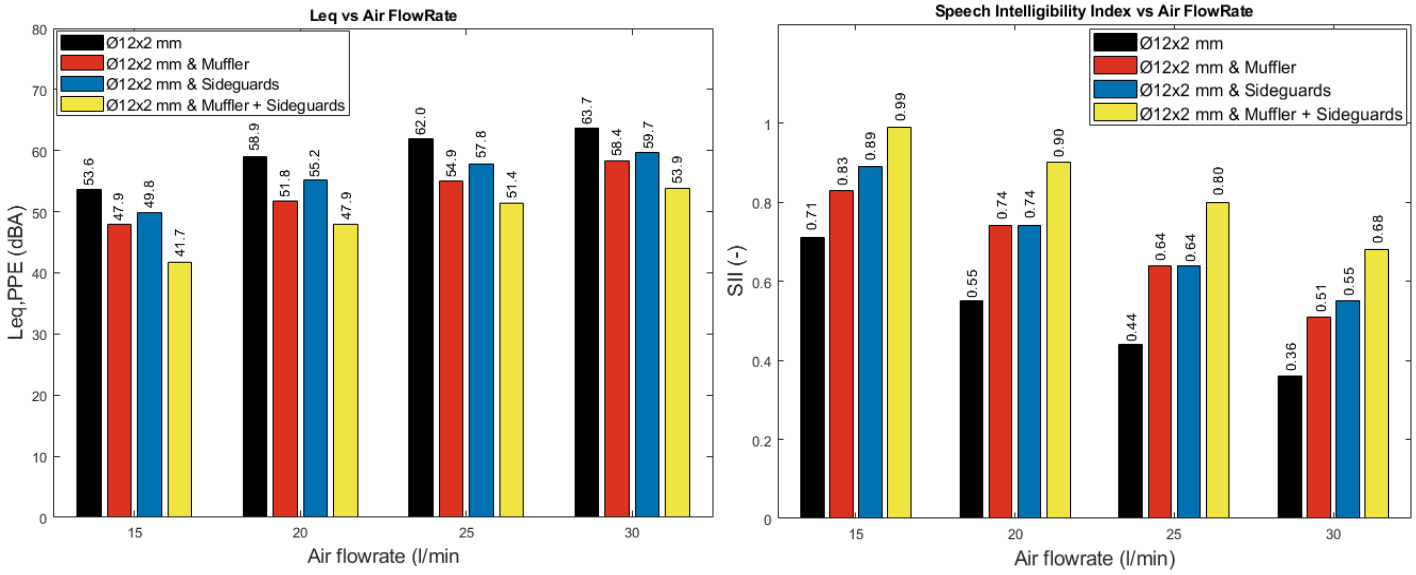

Figure 3.12: $L_{\mathrm{eq},PPE}$ and ***SII*** comparison for different mitigation strategies: Muffler vs Sideguards.

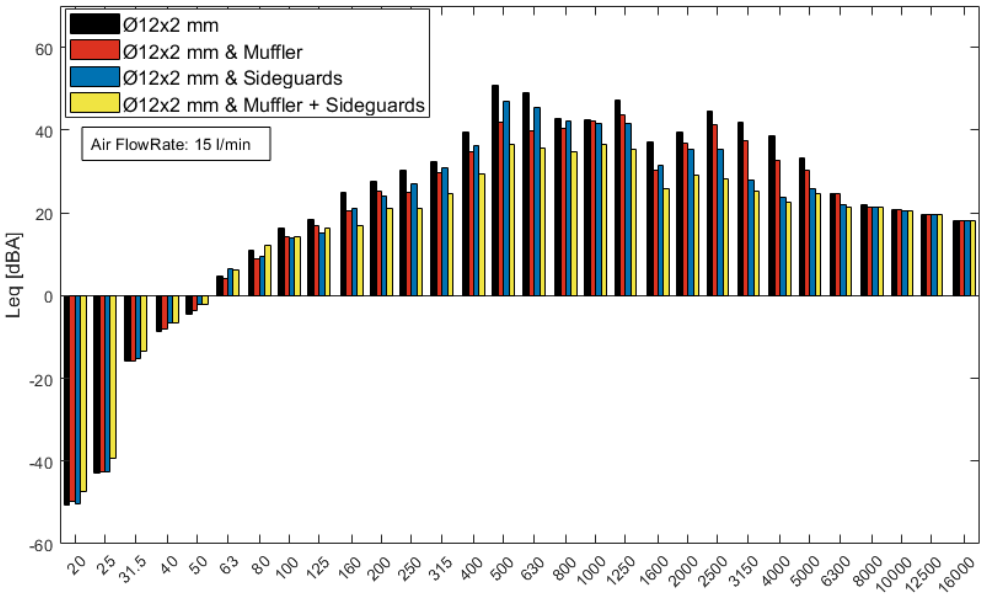

Figure 3.13: Spectra comparison for different mitigation strategies: Muffler vs Sideguards.

3.5. Tube Thickness and Insulation

To investigate the influence of tube thickness on noise generation, two tubes with the same interior diameter of 8 mm but different thicknesses (2 mm and 1 mm) were studied. The findings reveal that reducing the tube thickness enhances the acoustic performance of the PPE. Although the $L_{\mathrm{eq},PPE}$ for the 1 mm thickness tube was slightly higher at 25 and 30 l/min, the SII also exhibited an increase (Figure 3.14). Modifying the tube thickness can lead to changes in its acoustic properties, resulting in variations in the noise spectrum. Thinner tubes may offer better attenuation characteristics in mid-range frequency bands (Figure 3.15), which play a significant role in determining SII. The use of thinner tubes was further justified by the additional improvements in both noise levels and the SII achieved with the inclusion of the muffler and sideguards.

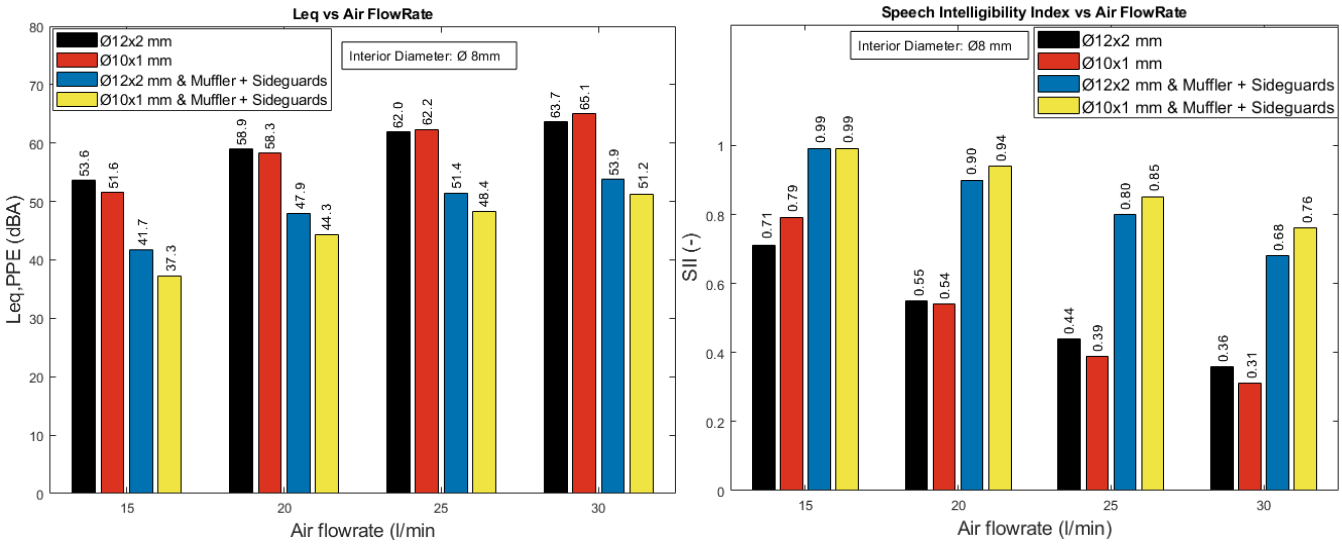

Figure 3.14: $L_{\mathrm{eq},PPE}$ and SII comparison for different tube thicknesses.

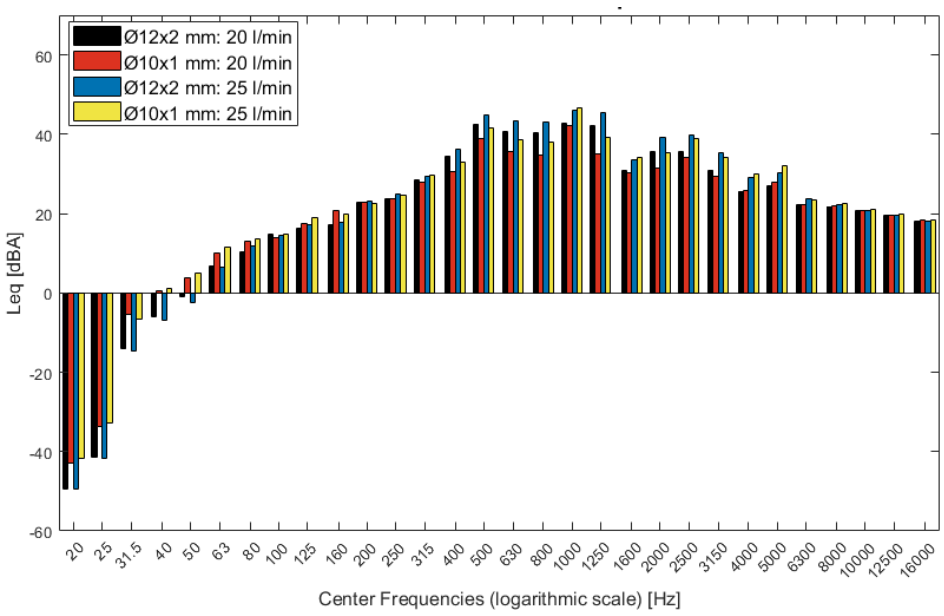

Figure 3.15: Spectra comparison for different tube thicknesses at varying air flowrates.

Further investigation was carried out by applying a 6 mm thickness insulation around the tube. This approach led to an increase in $L_{\mathrm{eq},PPE}$ and a decrease in SII (Figure 3.16). This amplification is seen across the spectra (Figure 3.17), which indicates that isolating the tubes might led to an amplification of noise propagation within them. Consequently, the higher noise levels reached the outlet at the jet slots and ultimately propagated to the user's ear.

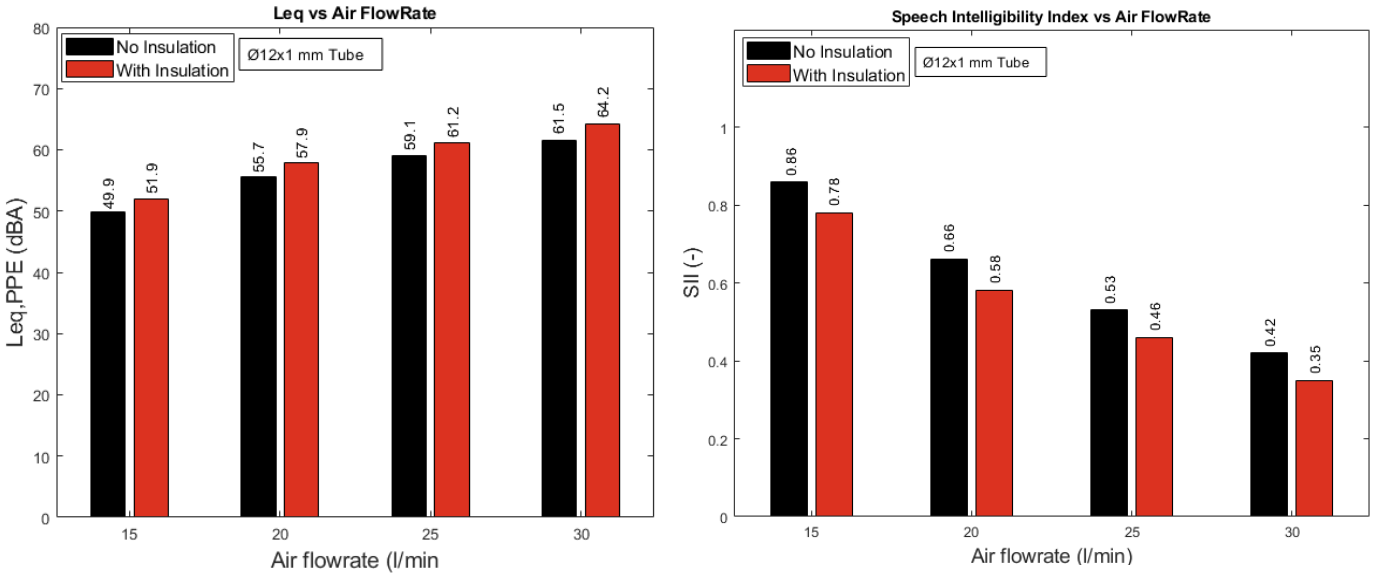

Figure 3.16: $L_{eq,PPE}$ and SII comparison: No Insulation vs With Insulation.

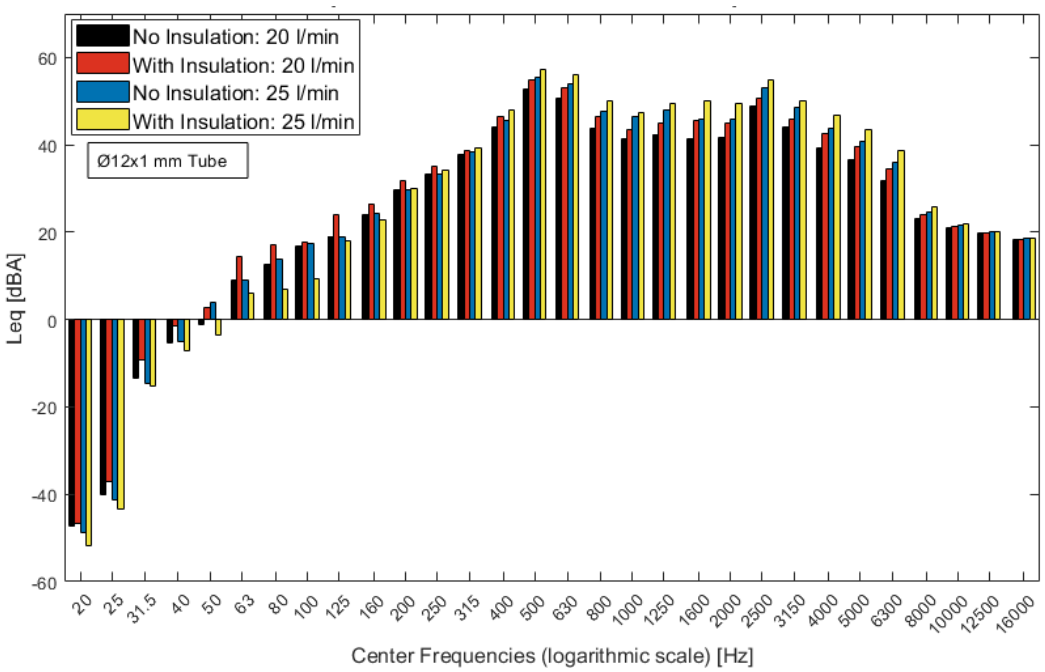

Figure 3.17: Impact of tube insulation on noise spectra.

3.6. Plenum Modifications

To address the direct impact of air on the plenum floor and its contribution to noise generation, modifications were implemented. One of these modifications involved placing a 3 mm height felt cushion pad on the plenum floor. The purpose was to create a softer barrier that would absorb sound waves energy and subsequently reduce noise levels. The results showed a decrease in the $L_{\mathrm{eq},PPE}$, indicating a reduction in noise levels (Figure 3.18). However, an increase in the mid-range frequencies in the spectra (Figure 3.19) resulted in decrease of the SII. As mentioned before, these frequencies carry greater weight in the SII calculation and are important for speech intelligibility. Although the cushion effectively reduced noise levels, the compromised SII suggests a negative impact on speech intelligibility, making this solution unsuitable in the present context.

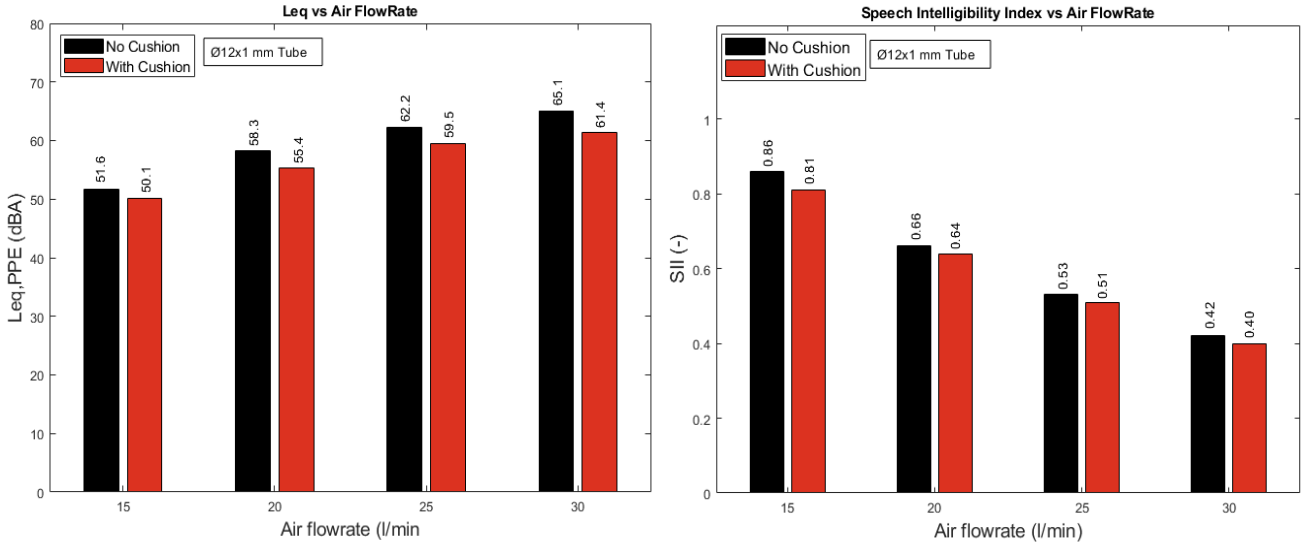

Figure 3.18: $L_{\mathrm{eq},PPE}$ and SII comparison: No Cushion vs With Cushion.

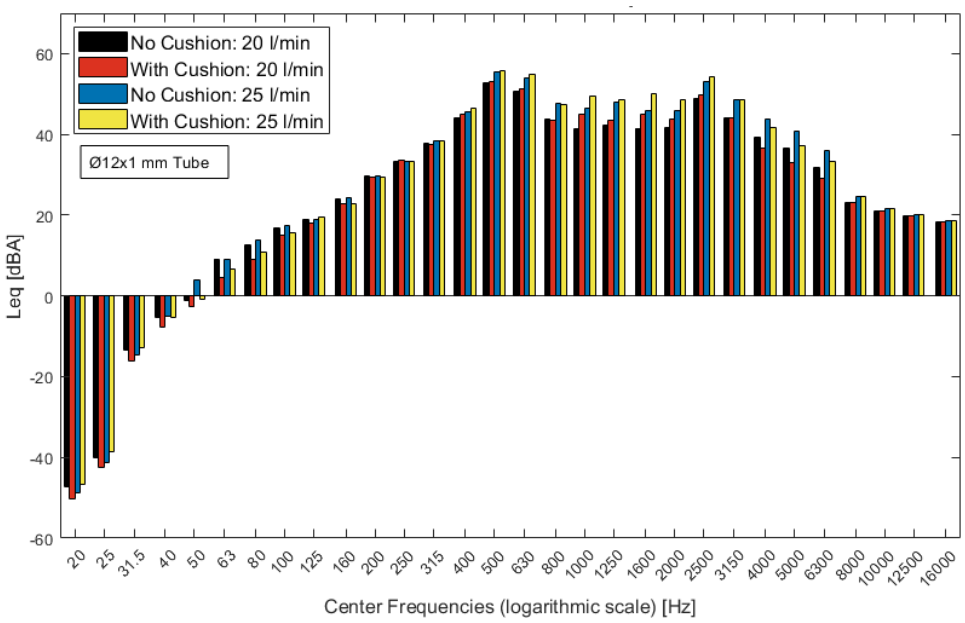

Figure 3.19: Impact of the plenum cushion on noise spectra.

Another strategy to mitigate air impact involved placing a 3D printed cone at the location where the air would impact the plenum floor (Figure 3.20). The technical drawing of the cone can be found in Appendix C.

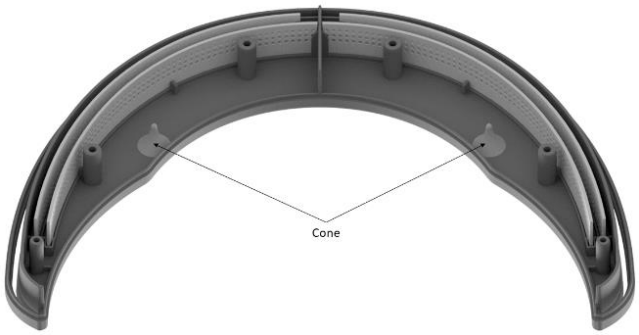

Figure 3.20: Cone assembly on the plenum floor

The cone acts as a diffuser, dispersing the air flow and minimising pressure fluctuations, thereby improving the distribution of air impact force compared to direct impact on the plenum floor. This improvement is evident from a Computational Fluid Dynamics (CFD) simulation made to compare the dynamic pressure fluctuations with and without the cone (Figure 3.21). Furthermore, the presence of the cone did not alter the velocity of the jet slots, ensuring the sealing effect remains intact. These findings confirm that integrating the cone is feasible without compromising the effectiveness of the PPE.

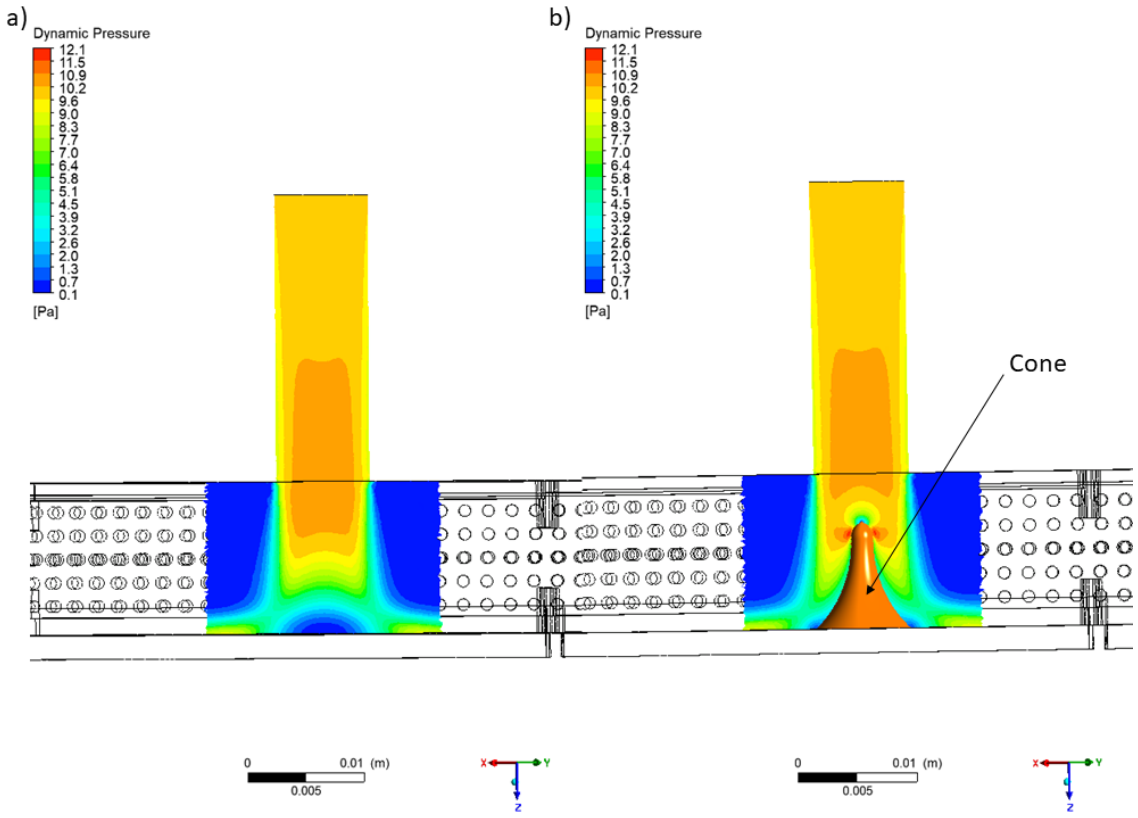

Figure 3.21: Comparison of dynamic pressure using CFD simulation: a) Without Cone and b) With Cone.

When integrating the cone and using the Ø10x1 mm tube, it resulted in decreased $L_{\mathrm{eq},PPE}$ and a general attenuation of frequency band levels (Figure 3.23), leading to increased *SII* values. In spite of that, when implementing the cone with the Ø12x1 mm tube, the results showed the opposite trend (Figure 3.22), making this solution not suitable for this tube diameter.

However, it is worth noting that despite the observed inverse trend for the Ø12x1 mm tube with the cone integration, the results still indicate the potential effectiveness of this solution when lower tube diameters are employed. Specifically, the $L_{\mathrm{eq},PPE}$ for the Ø10x1 mm tube with the cone and the Ø12x1 mm tube without the cone were relatively close to each other. The reduced mean air velocity in the Ø12x1 mm tube may result in less effective air distribution and turbulence within the plenum volume, leading to increased noise levels. This suggests that the cone integration may be more beneficial for lower tube diameters where the mean air velocity is higher.

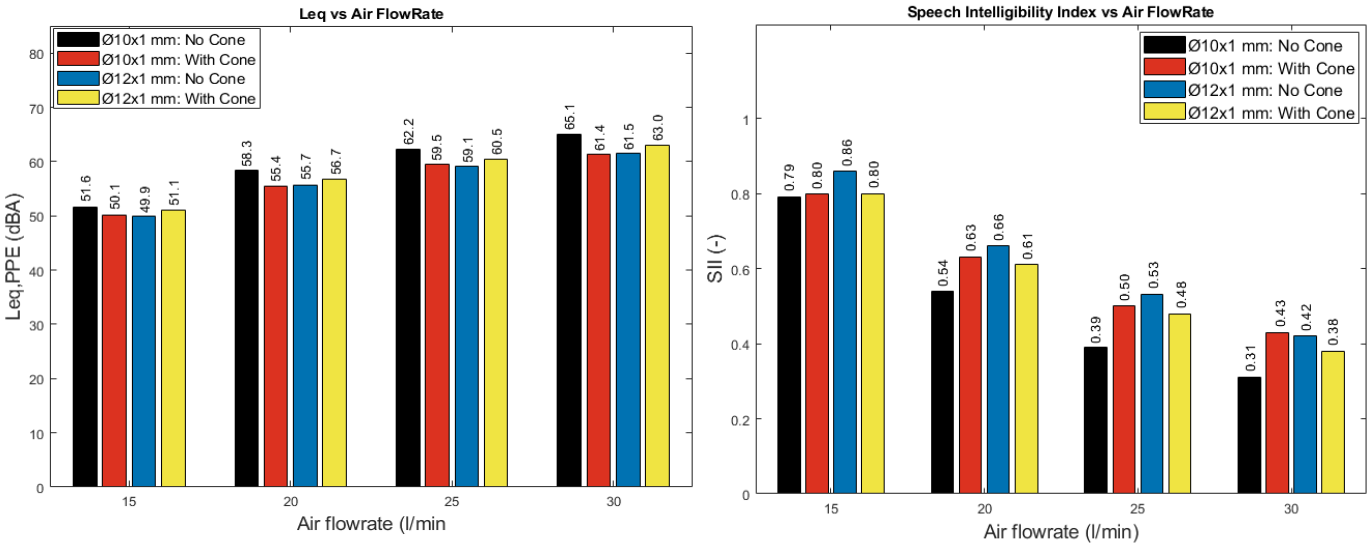

Figure 3.22: $L_{\mathrm{eq},PPE}$ and SII comparison: No Cone vs With Cone for different tube diameters.

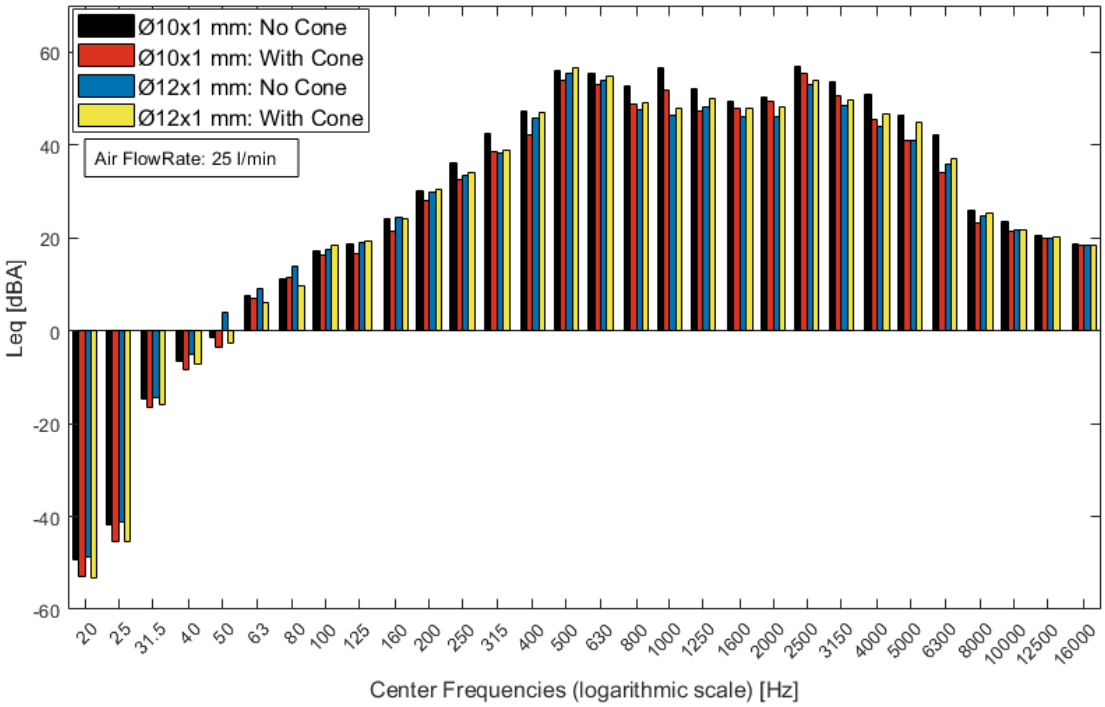

Figure 3.23: Impact of the plenum cone on noise spectra.

3.7. Splitter Design

The presence of a splitter in the airflow path can induce turbulence and contribute to noise generation. To address this issue, alternative splitter designs were developed and evaluated to assess their impact on noise production. One such design was the Ys (Y streamlined) splitter, a 3D printed part designed to minimise air disturbance. A visual comparison between the original Y splitter and the Ys splitter can be observed in Figure 3.24, with a technical drawing of the Ys splitter, available in Appendix D.

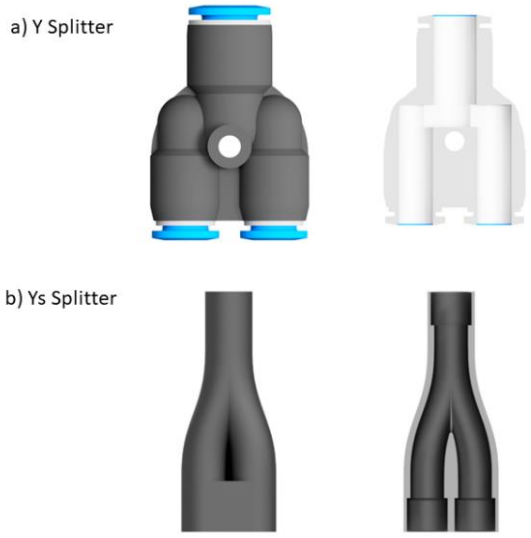

Figure 3.24: Splitter illustration: a) Y Splitter; b) Ys Splitter

However, the Ys splitter solution did not yield the expected results. The $L_{\mathrm{eq},PPE}$ increased by approximately 3 dBA across all air flowrates, and the *SII* also decreased (Figure 3.26). This decrease in acoustic performance is further supported by the spectra (Figure 3.27), which demonstrate notable increases in most frequency bands. These results led to the conclusion that the Ys splitter design facilitates the propagation of noise from upstream due to its reduced disturbance, which can decrease sound waves reflection back to the source.

Consequently, a new splitter design, known as the Reactive Muffler Splitter (RMS), was developed and 3D printed (Figure 3.25). Inspired by automotive exhaust mufflers, this design aims to reduce noise by reflecting a portion of the sound waves back to the source or within the chamber that houses the extended inlet and outlet tubes [60]. A technical drawing of the RMS is available in Appendix E

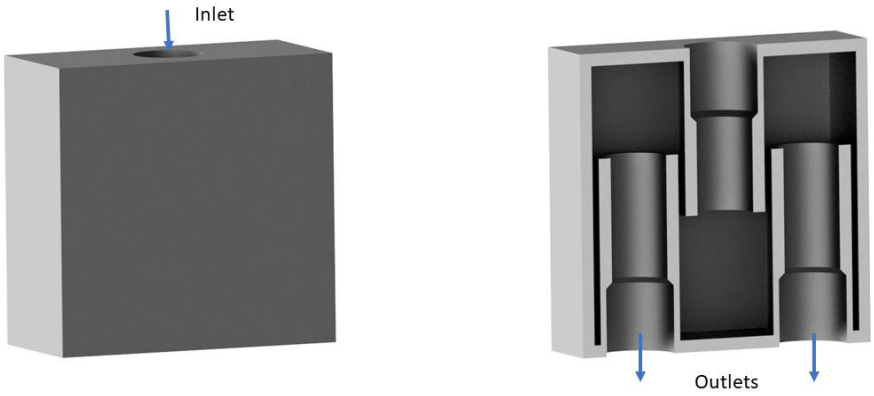

Figure 3.25: Reactive Muffler Splitter

The results demonstrate the potential effectiveness of the RMS when integrated into the system, as indicated by the decrease in $L_{\mathrm{eq},PPE}$ across all air flowrates and the corresponding increase in SII (Figure 3.26). The significant improvements in SII can be attributed to the spectra, which revealed significant attenuation of the critical mid-range frequencies (Figure 3.27), achieved by the new splitter design.

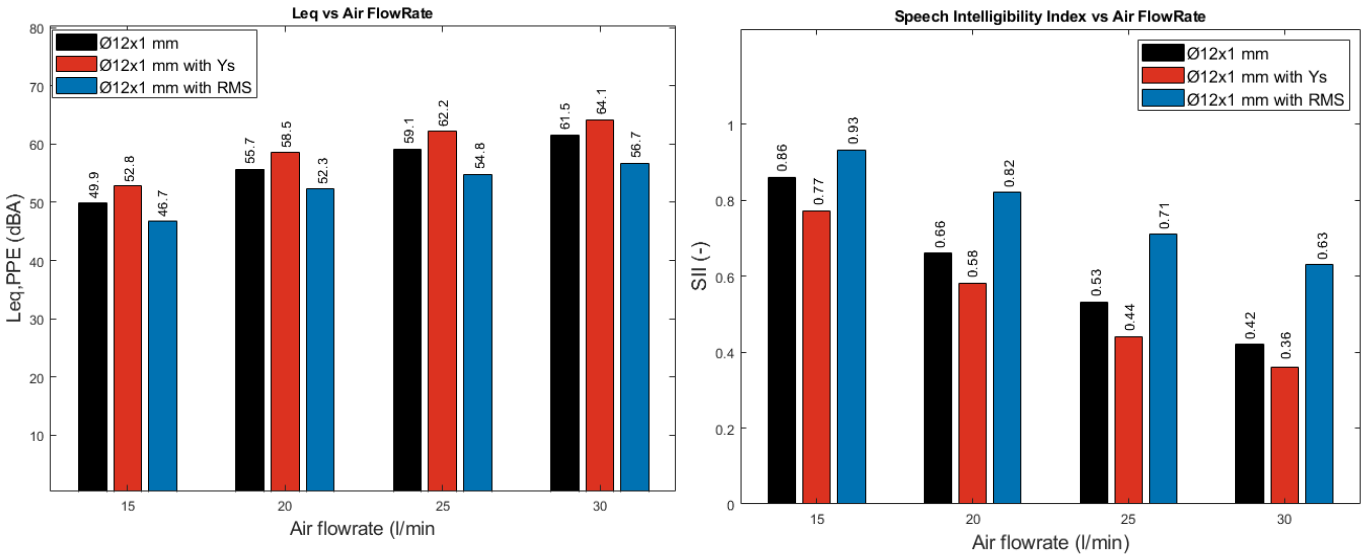

Figure 3.26: $L_{\mathrm{eq},PPE}$ and SII comparison for different splitter designs.

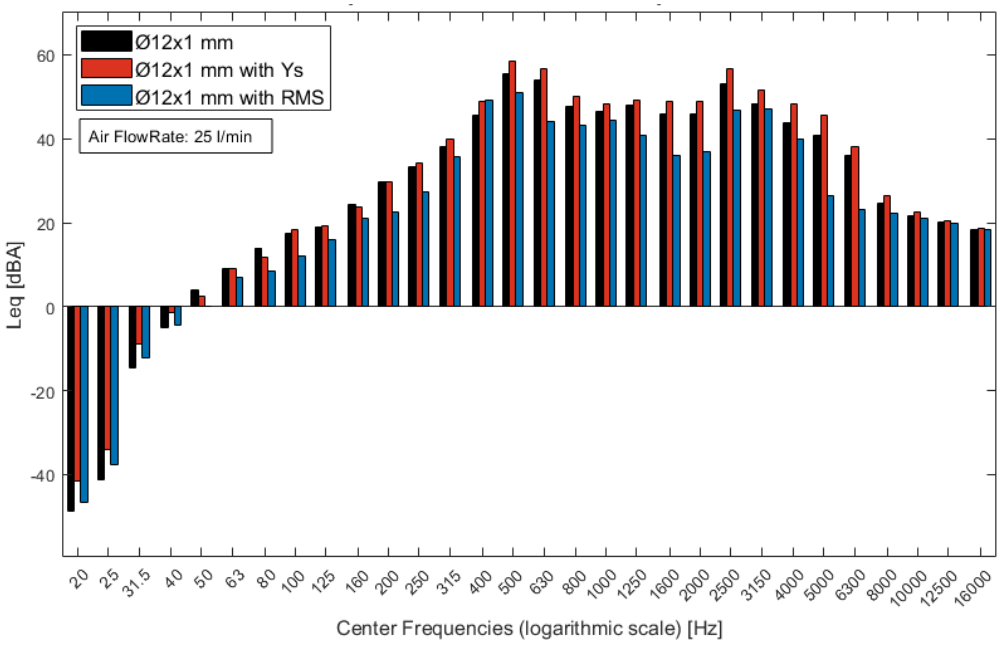

Figure 3.27: Spectra comparison for different splitter designs.

When incorporating the muffler and sideguards along with the RMS, the positive effects of the RMS on noise reduction were still observed. The integration of these components led to additional noise reduction, enabling the attainment of maximum *SII* values and close to 1.00 across all air flowrates (Figure 3.28). The spectra reveal a noticeable attenuation of mid-range frequencies, even in the presence of other add-ons (Figure 3.29). These results strongly support the integration of the RMS in the PPE configuration as it consistently reduces noise levels and significantly improves speech intelligibility.

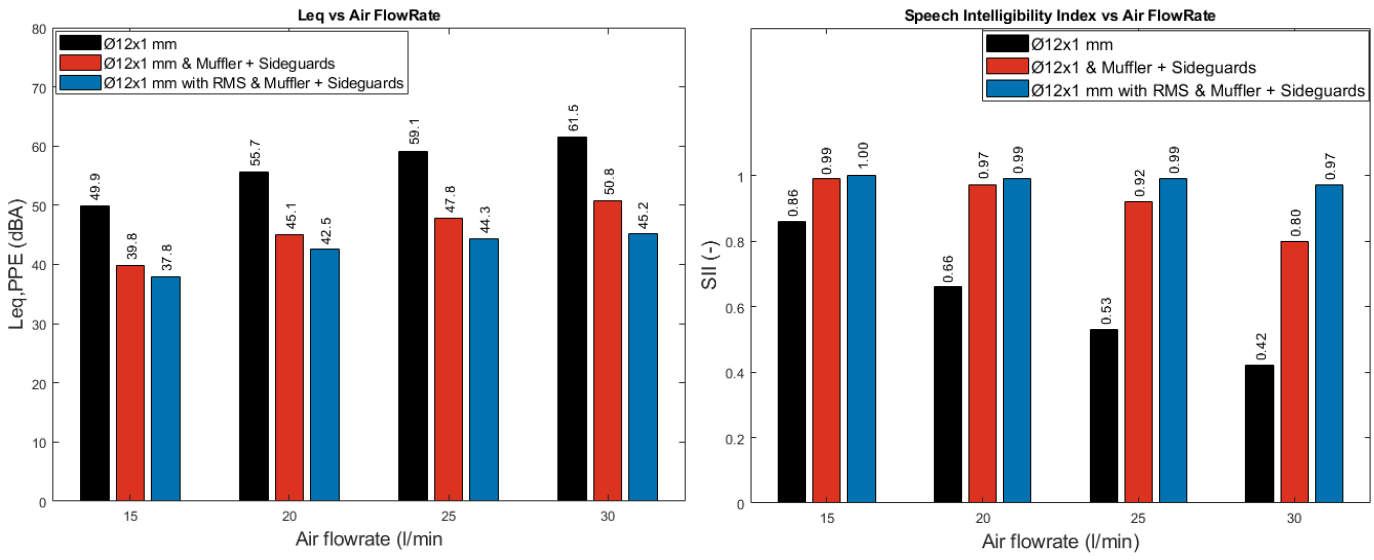

Figure 3.28: $L_{eq,PPE}$ and SII comparison of RMS with add-ons.

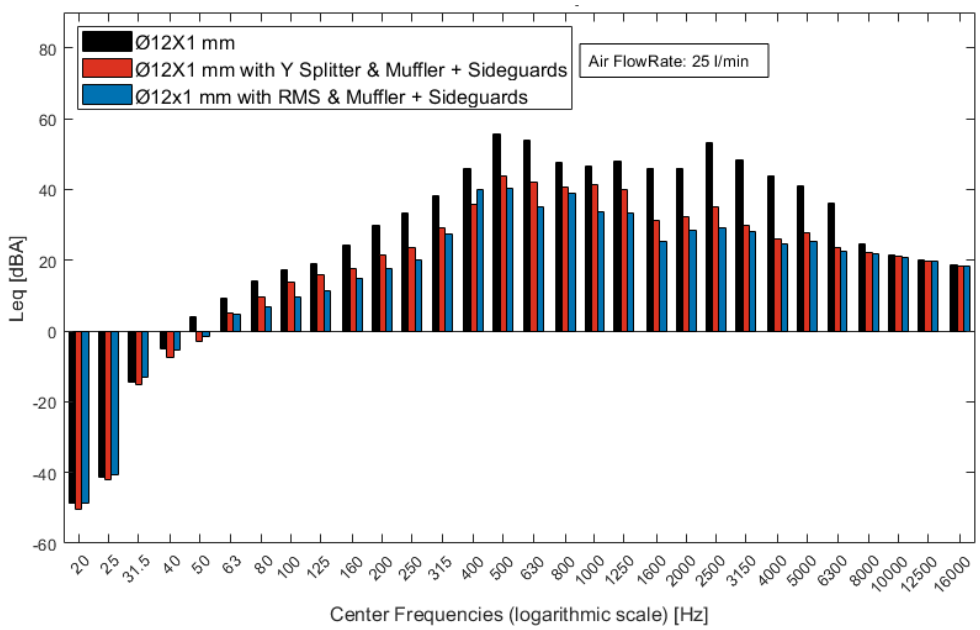

Figure 3.29: Spectra comparison of RMS with add-ons.

3.8. Final Prototype

Through a series of optimisations implemented during the study, significant improvements were achieved when comparing the initial solution to the final prototype. These optimisations resulted in a substantial reduction in noise levels, ranging from 20 to 30 dBA across all flow rates. The noise levels did not exceed 45.2 dBA, which is considered safe and falls well below the recommended occupational noise limits [41], [42].

Additionally, the Speech Intelligibility Index (*SII*) reached its maximum value of 1.00 and consistently maintained a proximity to that value for all flow rates, indicating excellent speech clarity and intelligibility (Figure 3.30). Spectral analysis revealed noticeable noise reduction across all frequency bands, with a more pronounced attenuation observed in the mid-range frequency bands crucial for speech comprehension (Figure 3.31). The distribution of noise levels across the spectrum was also well-balanced, addressing concerns of annoyance, mental performance degradation, and potential hearing impairment associated with increased frequency components [20], [24], [25], [27]–[29].

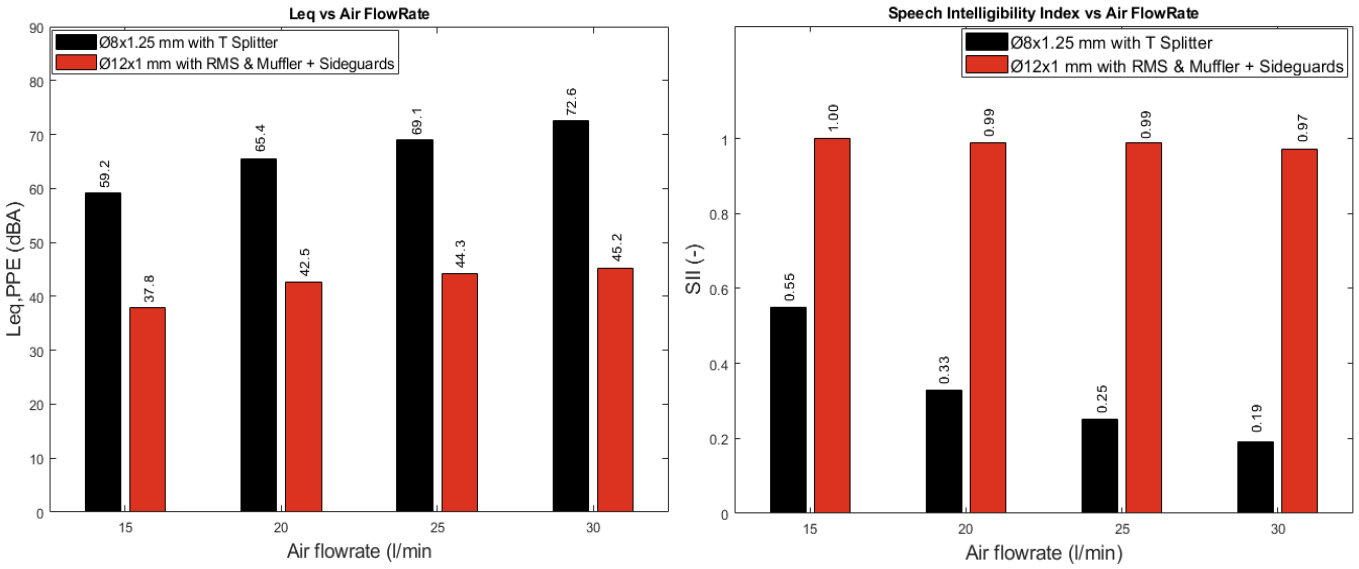

Figure 3.30: $L_{\mathrm{eq},PPE}$ and SII comparison: first and last PPE iteration.

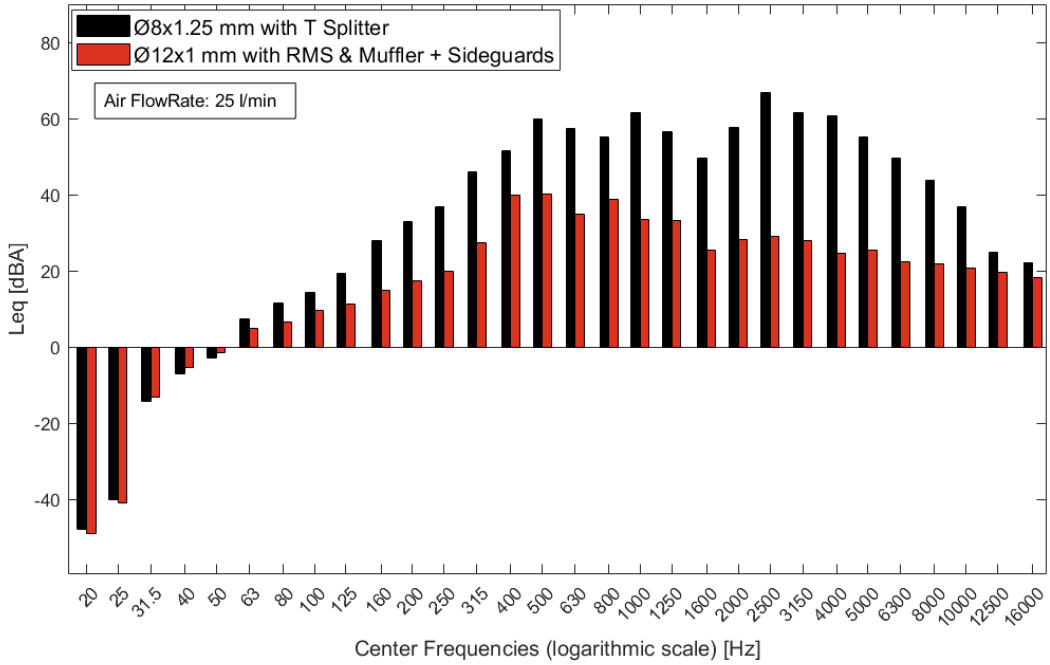

Figure 3.31: Spectra comparison: first and last PPE iteration.

3.9. PPE Impact on Speech

In addition to their primary purpose providing protection, Personal Protective Equipment (PPE) can also affect communication. These equipment items have the potential to attenuate speech levels, which can hinder effective communication. This becomes particularly problematic in work situations where clear speech is essential for carrying out procedures and maintaining optimal performance [7].

Initially, the influence of the PPE on the measured sound levels was assessed, as the noise produced by the air curtain can also cause speech masking. It was found that the white noise emitted by the speaker effectively masked the noise generated by the PPE in its most effective configuration considering an air flowrate of 30 l/min (Figure 3.32). Furthermore, the comparison of the one-third octave band spectra showed negligible differences between them, as illustrated in Figure 3.32.

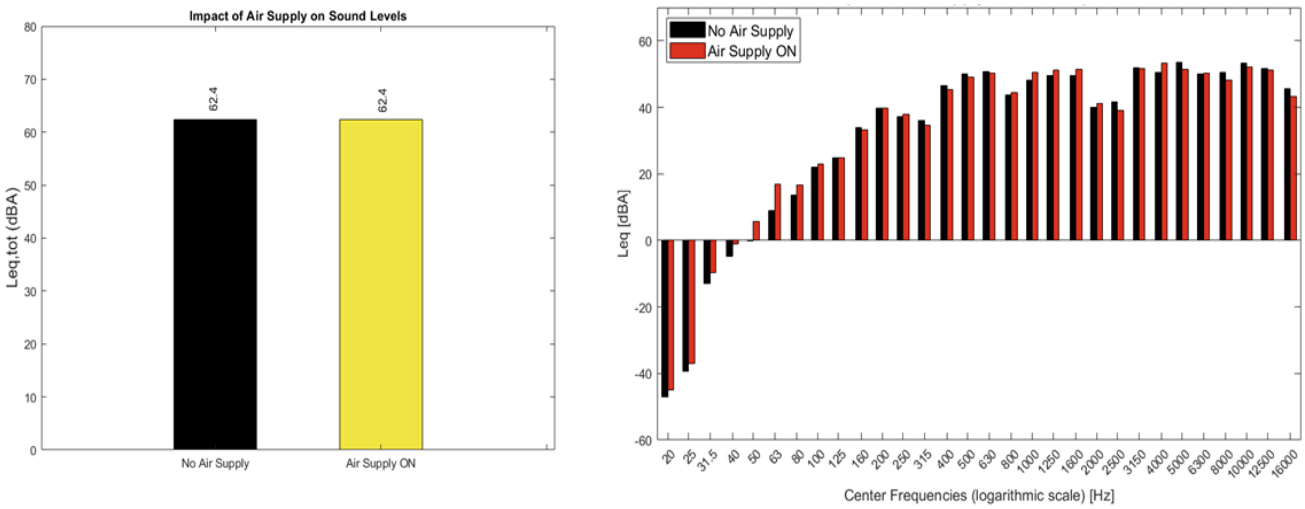

Figure 3.32: Effect of PPE air supply on ambient noise levels

The white noise emitted by the speaker was set to 67 dBA in the no mask condition. The attenuation of this sound signal observed for the surgical mask is consistent with the findings reported by Goldin *et al.* [61] with a reduction of approximately 3 dBA. Similarly, the FFP2 respirator demonstrated a comparable level of attenuation. In contrast, the VV4MC demonstrated a notable attenuation of almost 5 dBA (Figure 3.33). Analysing the spectra (Figure 3.34), there was an increase in frequency band levels between 200 Hz and 630 Hz, but a significant attenuation was observed between 800 Hz and 2000 Hz in the VV4MC spectrum. This attenuation in the critical frequency range for human hearing [37] may pose

a challenge to speech transmission, although the difference in attenuation between VV4MC and the other two PPE options did not exceed 3 dBA.

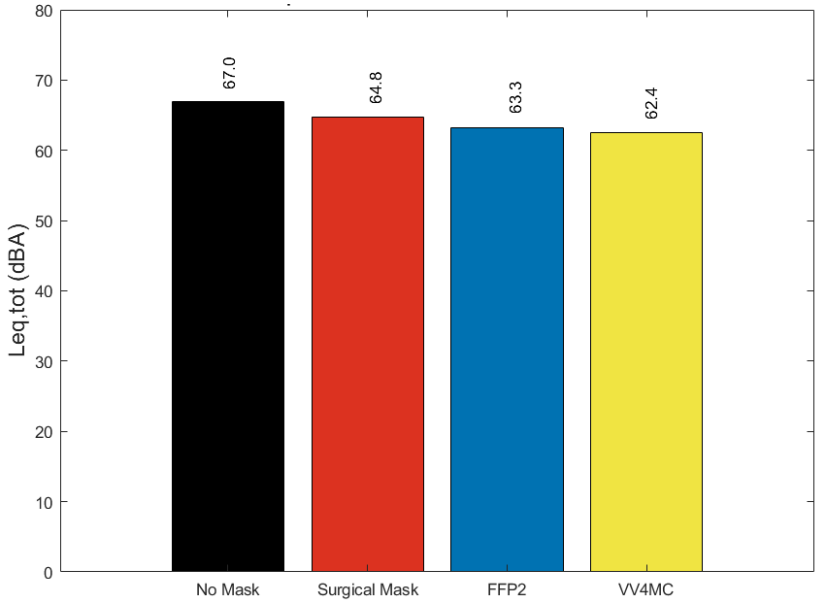

Figure 3.33: White noise attenuation of different types of PPE

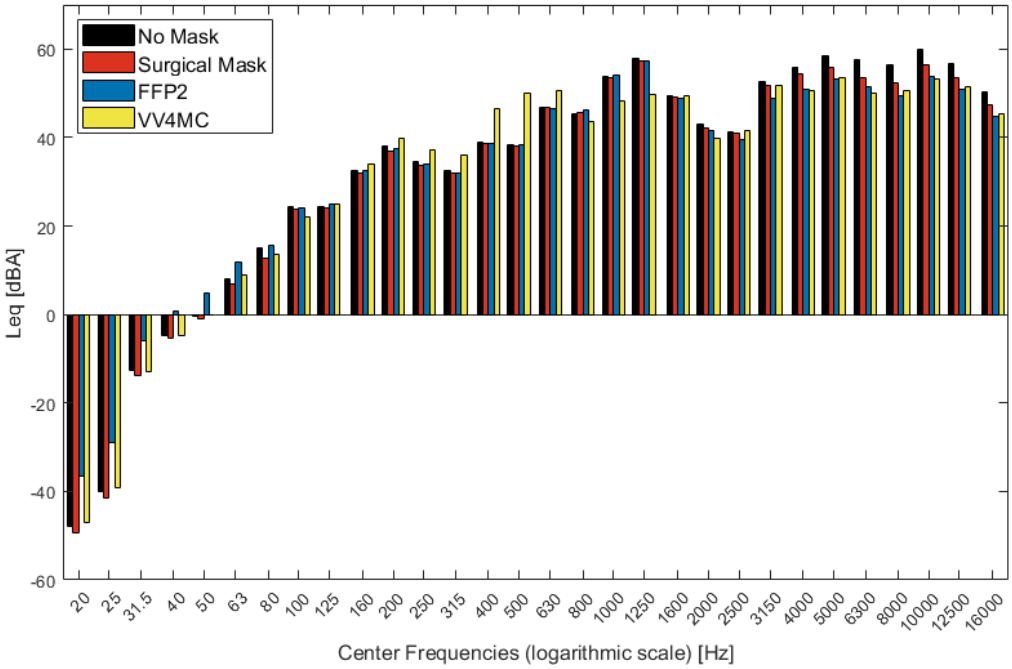

Figure 3.34: Spectra comparison for different types of PPE

4. CONCLUSIONS

This study was conducted as part of the VV4MC project, which aims to optimise the existing MASK4MC design. The main objective of the optimisation was to assess and improve the acoustic performance of the PPE as it inherently generated noise during operation. Various methods were employed, including measuring noise levels, conducting frequency analysis, and evaluating the Articulation Index (AI) and Speech Intelligibility Index (SII).

Several conclusions can be drawn from the results of the study. Firstly, it was observed that using the PPE without the air curtain did not have a significant impact on the ambient noise levels measured at the manikin's ear.

Then, with the air supply turned on, a decrease in the acoustic performance as the air flowrates increased was observed, which can be attributed to the higher mean velocity of the airflow. Additionally, it was found that increasing the internal diameter of the tubes resulted in an improvement in the acoustic performance.

The use of thicker tubes was found to be associated with a degradation in acoustic performance, likely due to changes in the acoustic properties of the tubes, as indicated by the observed changes in the frequency spectrum. Also, applying a 6 mm thickness insulation to the tubes, led to a degradation in acoustic performance. This was attributed to a greater propagation of noise from the air supply system through the tubes, resulting in higher noise levels at the manikin's ear.

Switching from a T-shaped to a Y-shaped splitter improved noise levels and speech intelligibility by reducing air flow disturbance and eliminating disruptive curved connections. The Ys splitter, which aimed to further reduce air flow disturbance, also allowed for increased noise propagation from the air supply system. Finally, implementing the RMS resulted in a significant improvement in the overall acoustic performance of the system, effectively reducing the propagated noise.

By integrating a muffler with a porous medium, inserted 1.5 meters upstream of the splitter, and implementing sideguards, notable reductions in noise levels and improvements in speech intelligibility were achieved. The muffler successfully attenuated noise propagated

through the tubes, while the sideguards acted as a physical barrier near the manikin's ear, effectively blocking noise emitted from the plenum outlets.

At the plenum, the addition of a 3 mm cushion felt pad on the plenum floor to mitigate noise generated by air impact, effectively reduced noise levels, yet it had a negative impact on speech intelligibility due to alterations in the frequency spectrum. The 3D printed cone effectiveness varied depending on the tube diameter, being more effective for smaller internal diameters and less effective for larger ones.

Based on these findings, it can be concluded that the primary source of noise is the air supply system. Implementing measures to attenuate this noise, decreasing its propagation through the tubes, and preventing it from reaching the plenum outlets, led to an improvement in acoustic performance.

Comparing the final solution to the initial one, notable reductions in noise levels of 20 to 30 dBA were observed across all flowrates. The noise levels remained below 45.2 dBA, well below the recommended limits. Moreover, the final solution exhibited excellent speech intelligibility, in contrast to the initial solution that had poor performance in this regard.

When assessing speech attenuation with white noise, the final prototype showed slightly inferior results compared to the surgical mask and FFP2 respirator, although the differences were not significant.

In future work, conducting tests in an anechoic room can enhance the evaluation of the prototype's acoustic performance by reducing ambient noise and minimising wall reflections. Usability tests in real working conditions are crucial for assessing user comfort, satisfaction, and overall usability of the PPE. Including survey testing within these usability tests would gather valuable feedback to refine and improve the design and functionality of the PPE.

REFERENCES

[1] W. E. Bischoff *et al.*, "Detection of Measles Virus RNA in Air and Surface Specimens in a Hospital Setting," *J. Infect. Dis.*, vol. 213, no. 4, pp. 600–603, Feb. 2016, doi: 10.1093/INFDIS/JIV465.

[2] R. Tellier, "Review of Aerosol Transmission of Influenza A Virus," *Emerg. Infect. Dis.*, vol. 12, no. 11, p. 1657, 2006, doi: 10.3201/EID1211.060426.

[3] H. Kulkarni, C. M. Smith, D. D. H. Lee, R. A. Hirst, A. J. Easton, and C. O'Callaghan, "Evidence of respiratory syncytial virus spread by aerosol time to revisit infection control strategies?," *Am. J. Respir. Crit. Care Med.*, vol. 194, no. 3, pp. 308–316, 2016, doi: 10.1164/rccm.201509-1833OC.

[4] S. L. Inhorn, "Aerosol Transmission of Rhinovirus Colds," *Artic. J. Infect. Dis.*, 1987, doi: 10.1093/infdis/156.3.442.

[5] M. Marani, G. G. Katul, W. K. Pan, and A. J. Parolari, "Intensity and frequency of extreme novel epidemics," *Proc. Natl. Acad. Sci. U. S. A.*, vol. 118, no. 35, p. e2105482118, Aug. 2021, doi: 10.1073/PNAS.2105482118/SUPPL_FILE/PNAS.2105482118.SAPP.PDF.

[6] K. E. Jones *et al.*, "Global trends in emerging infectious diseases," *Nat. 2008 4517181*, vol. 451, no. 7181, pp. 990–993, Feb. 2008, doi: 10.1038/nature06536.

[7] Y. Li *et al.*, "Effects of wearing N95 and surgical facemasks on heart rate, thermal stress and subjective sensations," *Int. Arch. Occup. Environ. Health*, vol. 78, no. 6, pp. 501–509, Jul. 2005, doi: 10.1007/S00420-004-0584-4/FIGURES/6.

[8] B. V. Shenal, L. J. Radonovich, J. Cheng, M. Hodgson, and B. S. Bender, "Discomfort and exertion associated with prolonged wear of respiratory protection in a health care setting," *J. Occup. Environ. Hyg.*, vol. 9, no. 1, pp. 59–64, Jan. 2012, doi: 10.1080/15459624.2012.635133.

[9] M. Abboah-Offei, Y. Salifu, B. Adewale, J. Bayuo, R. Ofosu-Poku, and E. B. A. Opare-Lokko, "A rapid review of the use of face mask in preventing the spread of COVID-19," *Int. J. Nurs. Stud. Adv.*, vol. 3, Nov. 2021, doi: 10.1016/J.IJNSA.2020.100013.

[10] D. K. Chu *et al.*, "Physical distancing, face masks, and eye protection to prevent

person-to-person transmission of SARS-CoV-2 and COVID-19: a systematic review and meta-analysis," *Lancet (London, England)*, vol. 395, no. 10242, pp. 1973–1987, Jun. 2020, doi: 10.1016/S0140-6736(20)31142-9.

[11] J. T. J. Ju, L. N. Boisvert, and Y. Y. Zuo, "Face masks against COVID-19: Standards, efficacy, testing and decontamination methods," *Adv. Colloid Interface Sci.*, vol. 292, p. 102435, Jun. 2021, doi: 10.1016/J.CIS.2021.102435.

[12] J. Brainard *et al.*, "A mixed methods study on effectiveness and appropriateness of face shield use as COVID-19 PPE in middle income countries," *Am. J. Infect. Control*, vol. 50, no. 8, pp. 878–884, Aug. 2022, doi: 10.1016/j.ajic.2022.01.019.

[13] H. Clack, "Personal cold plasma 'air curtain' design for COVID-19 protection moves forward | University of Michigan News," 2020. https://news.umich.edu/personal-cold-plasma-air-curtain-design-for-covid-19-protection-moves-forward/ (accessed Mar. 14, 2023).

[14] X. Wei, D. Yi, W. Xie, J. Gao, and L. Lv, "Protection against inhalation of gaseous contaminants in industrial environments by a personalized air curtain," *Build. Environ.*, vol. 206, p. 108343, Dec. 2021, doi: 10.1016/J.BUILDENV.2021.108343.

[15] D. Keisar, A. Garzozi, M. Shoham, and D. Greenblatt, "Development and evaluation of a fluidic facemask for airborne transmission mitigation," *Exp. Therm. Fluid Sci.*, vol. 141, p. 110777, Feb. 2023, doi: 10.1016/J.EXPTHERMFLUSCI.2022.110777.

[16] J. Manne, "Air curtain device," Apr. 07, 2003

[17] Susan G. Danisch, Michael R. Berrigan, and Patrick H. Carey Jr., "PROTECTIVE SYSTEM FOR FACE AND RESPIRATORY PROTECTION," Dec. 16, 2000

[18] S. . G. Pais, J.; Jesus, L.; Silva, H.; Lopes, A.; Ramos, J.; Costa, J. J.; Gameiro da Silva, M.; Martinho, N.; Rosa, N.; Matos, "Viseira de vedação aerodinâmica. Modelo de utilidade como EPI de categoria III, Ref. DP/02/2021/76885. Desenvolvido no âmbito do projeto Mask4MC – Mask for Medical Care (Dispositivo de proteção individual para cuidados médicos), projeto em copromoção liderado pela SETsa - Sociedade de Engenharia e Transformação S.A. e tendo com copromotores a ADAI - Associação para o Desenvolvimento da Aerodinâmica Industrial e a FMUC - Faculdade de Medicina da Universidade de Coimbra." 2021 [Online]. Available: https://patents.google.com/patent/PT12042U/pt?q=(Viseira+de+vedação+aerodinâmica)&oq=Viseira+de+vedação+aerodinâmica

[19] M. L. Munjal, *Noise and vibration control*, vol. 3. World Scientific Publishing Co. Pte. Ltd., 2013. doi: https://doi.org/10.1142/8614.

[20] World Health Organization, "Occupational noise: assessing the burden of disease from work-related hearing impairment at national and local levels," *Environ. Burd. Dis. Ser.*, pp. 1–33, 2004, Accessed: Mar. 06, 2023. [Online]. Available: https://apps.who.int/iris/handle/10665/43001?search-result=true&query=OCCUPATIONAL+NOISE&scope=%2F&filtertype_0=dateIssued&filter_relational_operator_0=equals&filter_0=%5B2000+TO+2023%5D&rpp=10&sort_by=score&order=desc

[21] J. C. Setcos and A. Mahyuddin, "Noise Levels Encountered in Dental Clinical and Laboratory Practice.," *Int. J. Prosthodont.*, vol. 11, no. 2, pp. 150-150–157, 1998, [Online]. Available: https://search.ebscohost.com/login.aspx?direct=true&db=ddh&AN=37215254&site=eds-live

[22] H. M. Elmehdi, "Assessing acoustic noise levels in dental clinics and its link to dental anxiety and fear among UAE population," in *20th International Congress on Acoustics 2010, ICA 2010 - Incorporating Proceedings of the 2010 Annual Conference of the Australian Acoustical Society*, 2010, vol. 3, pp. 2038–2041.

[23] K. W. Ma, H. M. Wong, and C. M. Mak, "Dental environmental noise evaluation and health risk model construction to dental professionals," *Int. J. Environ. Res. Public Health*, vol. 14, no. 9, Sep. 2017, doi: 10.3390/ijerph14091084.

[24] T. Y. Chang, C. S. Liu, L. H. Young, V. S. Wang, S. E. Jian, and B. Y. Bao, "Noise frequency components and the prevalence of hypertension in workers," *Sci. Total Environ.*, vol. 416, pp. 89–96, Feb. 2012, doi: 10.1016/j.scitotenv.2011.11.071.

[25] M. Pawlaczyk-Łuszczyńska, A. Dudarewicz, M. Waszkowska, W. Szymczak, and M. Śliwińska-Kowalska, "The impact of low frequency noise on human mental performance," *Int. J. Occup. Med. Environ. Health*, vol. 18, no. 2, pp. 185–198, 2005, [Online]. Available: https://pubmed.ncbi.nlm.nih.gov/16201210/

[26] "Deafness and hearing loss," Accessed: Mar. 09, 2023. [Online]. Available: https://www.who.int/news-room/fact-sheets/detail/deafness-and-hearing-loss

[27] K. Persson Waye and R. Rylander, "The prevalence of annoyance and effects after long-term exposure to low-frequency noise," *J. Sound Vib.*, vol. 240, no. 3, pp. 483–

497, Feb. 2001, doi: 10.1006/jsvi.2000.3251.

[28] Y. Huang, G. Di, Y. Zhu, Y. Hong, and B. Zhang, "Pair-wise comparison experiment on subjective annoyance rating of noise samples with different frequency spectrums but same A-weighted level," *Appl. Acoust.*, vol. 69, no. 12, pp. 1205–1211, Dec. 2008, doi: 10.1016/J.APACOUST.2007.10.006.

[29] M. Pawlaczyk-Luszczynska, A. Dudarewicz, W. Szymczak, and M. Sliwinska-Kowalska, "Evaluation of annoyance from low frequency noise under laboratory conditions," *Noise Heal.*, vol. 12, no. 48, pp. 166–181, Jul. 2010, doi: 10.4103/1463-1741.64974.

[30] I. Alimohammadi and H. Ebrahimi, "Comparison between effects of low and high frequency noise on mental performance," *Appl. Acoust.*, vol. 126, pp. 131–135, Nov. 2017, doi: 10.1016/j.apacoust.2017.05.021.

[31] N. Rosa *et al.*, "Experimental and numerical evaluation of a new visor concept with aerodynamic sealing to protect medical professionals from contaminated droplets and aerosols," *Indoor Air*, vol. 32, no. 9, 2022, doi: 10.1111/ina.13114.

[32] D. R. Raichel and U. J. Hansen, *The Science and Applications of Acoustics*, 2nd ed., vol. 114, no. 1. Springer Science+Business Media, Inc., 2003. doi: 10.1121/1.1582438.

[33] International Organization for Standardization, *ISO 80000-8:2020(en) Quantities and units — Part 8: Acoustics*, vol. 2. 2020.

[34] G. M. Ballou, *Handbook for sound engineers, Fourth edition*. 2015. doi: 10.4324/9780203758281.

[35] International Organization for Standardization, *ISO/TR 25417:2007(en) Acoustics — Definitions of basic quantities and terms*, vol. 3. 2007.

[36] International Organization for Standardization, *ISO 3740:2019(en) Acoustics — Determination of sound power levels of noise sources — Guidelines for the use of basic standards*. 2019.

[37] J. G. Švec and S. Granqvist, "Tutorial and guidelines on measurement of sound pressure level in voice and speech," *J. Speech, Lang. Hear. Res.*, vol. 61, no. 3, pp. 441–461, Mar. 2018, doi: 10.1044/2017_JSLHR-S-17-0095.

[38] International Organization for Standardization, *ISO 16032:2004(en), Acoustics — Measurement of sound pressure level from service equipment in buildings — Engineering method*.

[39] International Electrotechnical Commission, *IEC 61672-1:2013, Electroacoustics - Sound level meters - Part 1: Specifications*. 2013.

[40] C. E. Wilson, T. K. Vaidyanathan, W. R. Cinotti, S. M. Cohen, and S. J. Wang, "Hearing-damage Risk and Communication Interference in Dental Practice," *J. Dent. Res.*, vol. 69, no. 2, pp. 489–493, Nov. 1990, doi: 10.1177/00220345900690021401.

[41] EU-OSHA, *Directive 2003/10/EC - noise | Safety and health at work EU-OSHA*. 2021. Accessed: May 22, 2023. [Online]. Available: https://osha.europa.eu/en/legislation/directives/82

[42] W. Murphy and J. Franks, "NIOSH Criteria for a Recommended Standard: Occupational Noise Exposure, Revised Criteria 1998," *J. Acoust. Soc. Am. - J ACOUST SOC AMER*, vol. 111, p. 2397, 2002, Accessed: May 22, 2023. [Online]. Available: https://blogs.cdc.gov/niosh-science-blog/2016/02/08/noise/

[43] J.-L. Tolliday, "What are A, C & Z Frequency Weightings? - NoiseNews," *Noise Meas.*, 2020, Accessed: Feb. 28, 2023. [Online]. Available: https://www.cirrusresearch.co.uk/blog/2020/03/what-are-a-c-z-frequency-weightings/

[44] L. E. Kinsler, A. R. Frey, A. B. Coppens, and J. V. Sanders, *Fundamentals of Acoustics*, 4th ed. John Wiley & Sons, Inc., 2000.

[45] H. Künkel, "Frequency analysis.," *Electroencephalography and clinical neurophysiology. Supplement*, no. 34. pp. 147–149, 1978. doi: 10.1201/9781315219080-6.

[46] J. Sinay, M. Balážiková, M. Dulebová, Š. Markulik, and Z. Kotianová, "Measurement of low-frequency noise during CNC machining and its assessment," *Meas. J. Int. Meas. Confed.*, vol. 119, pp. 190–195, Apr. 2018, doi: 10.1016/j.measurement.2018.02.004.

[47] *IEC 61260-2:2016+AMD1:2017, Electroacoustics - Octave-band and fractional-octave band filters - Part 2: Pattern evaluation tests*. 2017.

[48] N. R. French and J. C. Steinberg, "Factors Governing the Intelligibility of Speech Sounds," *J. Acoust. Soc. Am.*, vol. 19, no. 1, pp. 90–119, 1947, doi: 10.1121/1.1916407.

[49] K. D. Kryter, "Methods for the Calculation and Use of the Articulation Index," *J. Acoust. Soc. Am.*, vol. 34, no. 11, p. 1689, Jul. 1962, doi: 10.1121/1.1909094.

[50] B. Kelechava, "Speech Intelligibility Index - ANSI Blog," *Am. Natl. Stand. Inst.*, 2016, Accessed: Feb. 28, 2023. [Online]. Available: https://blog.ansi.org/2016/06/speech-

intelligibility-index/#gref

[51] S. M. R. Taghavi, G. Mohammadkhani, and H. Jalilvand, "Speech Intelligibility Index: A Literature Review," *Audit. Vestib. Res.*, vol. 31, no. 3, pp. 148–157, 2022, doi: 10.18502/avr.v31i3.9861.

[52] American National Standards Institute, *ANSI/ASA S3.5-1997 (R2020), Methods For Calculation Of The Speech Intelligibility Index*.

[53] M. C. G. Silva, "Sound Measuring Virtual Instruments," in *Rev 2007: 4th International Conference on Remote Engineering and Virtual Instrumentation*, 2007, pp. 1–3.

[54] M. C. G. da Silva and M. L. O. S. Mateus, "Desenvolvimento de um conjunto de aplicações computacionais para emolução de equipamentos de medição e análise sonora," in *V Congresso Ibérico de Acústica, Accoustics European Symposium*, 2008.

[55] M. C. G. da Silva, "Virtual Laboratories for a Course on Indoor Environmental Quality," *Spec. Issue Int. J. Emerg. Technol. Learn.*, vol. 5, no. 6, p. 20, 2009, doi: 10.3991/ijoe.v5s2.1107.

[56] International Electrotechnical Commission, *IEC 60942:2017 RLV, Electroacoustics - Sound calibrators*. 2017.

[57] N. Rosa, A. R. Gaspar, J. J. Costa, A. G. Lopes, J. Sabino Pais, and M. Gameiro da Silva, "Experimental assessment of an air curtain-sealed personal protective equipment for medical care: influence of breathing and thermal plume," *Exp. Therm. Fluid Sci.*, p. 110955, May 2023, doi: 10.1016/J.EXPTHERMFLUSCI.2023.110955.

[58] R. A. Scott, "The absorption of sound in a homogeneous porous medium," *Proc. Phys. Soc.*, vol. 58, no. 2, p. 165, Mar. 1946, doi: 10.1088/0959-5309/58/2/303.

[59] L. Cao, Q. Fu, Y. Si, B. Ding, and J. Yu, "Porous materials for sound absorption," *Compos. Commun.*, vol. 10, pp. 25–35, Dec. 2018, doi: 10.1016/J.COCO.2018.05.001.

[60] J. H. Chaudhri, B. S. Patel, and S. A. Shah, "Muffler Design for Automotive Exhaust Noise Attenuation-A Review," *J. Eng. Res. Appl. www.ijera.com*, vol. 4, no. 1, pp. 220–223, 2014, Accessed: May 15, 2023. [Online]. Available: www.ijera.com

[61] A. Goldin, B. Weinstein, and N. Shiman, "How Do Medical Masks Degrade Speech Reception? - The Hearing Review – a MEDQOR brand," *Hear. Rev.*, vol. 27, no. 5, pp. 8–9, 2020, [Online]. Available: https://hearingreview.com/hearing-loss/health-wellness/how-do-medical-masks-degrade-speech-reception

APPENDIX A

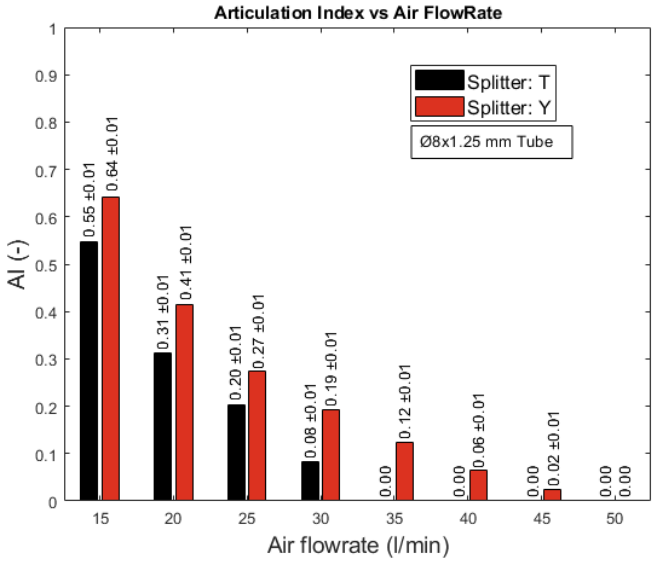

Figure A.1: AI for different splitters and air flowrates.

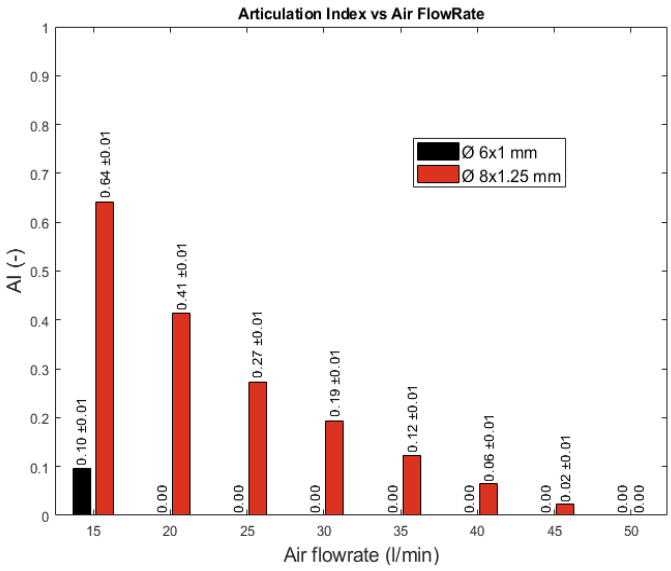

Figure A.2: AI for different tube diameters and air flowrates.

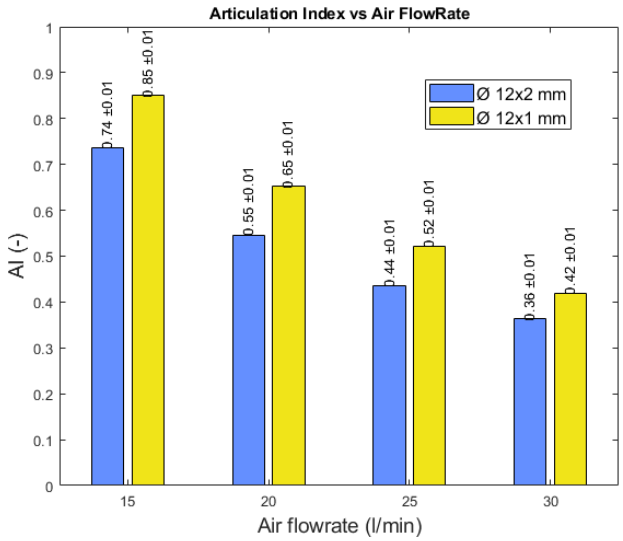

Figure A.3: AI for different tube diameters and air flowrates.

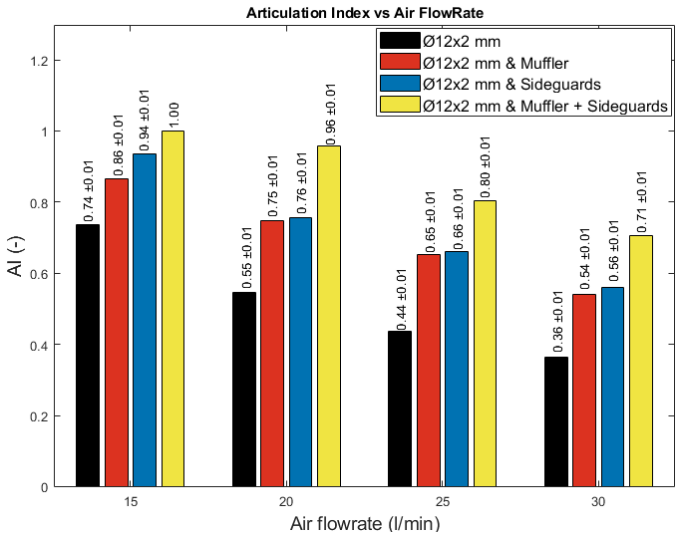

Figure A.4: AI comparison for different mitigation strategies: Muffler vs Sideguards.

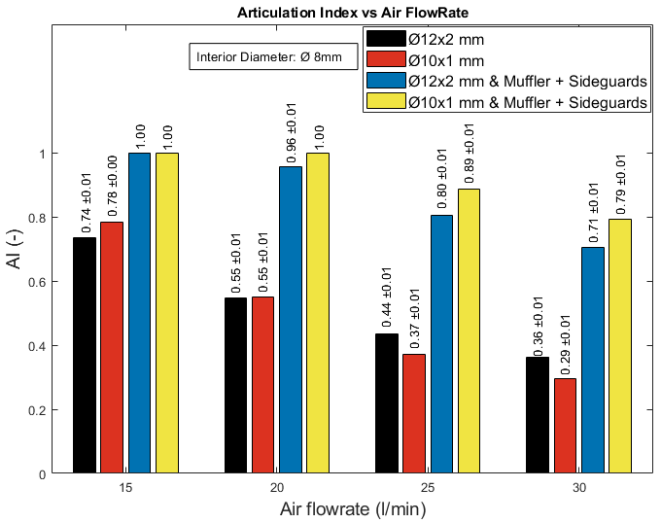

Figure A.5: AI comparison for different tube thicknesses.

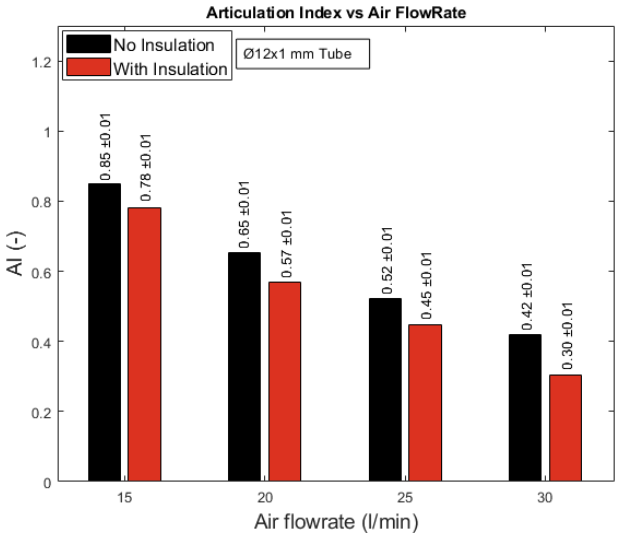

Figure A.6: AI comparison: No Insulation vs With Insulation.

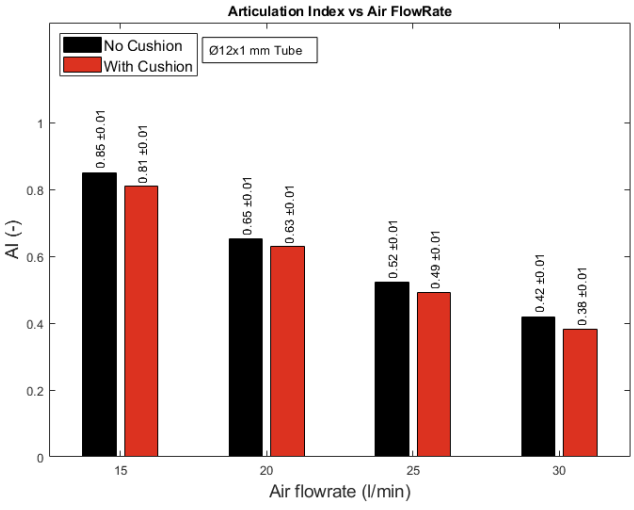

Figure A.7: AI comparison: No Cushion vs With Cushion.

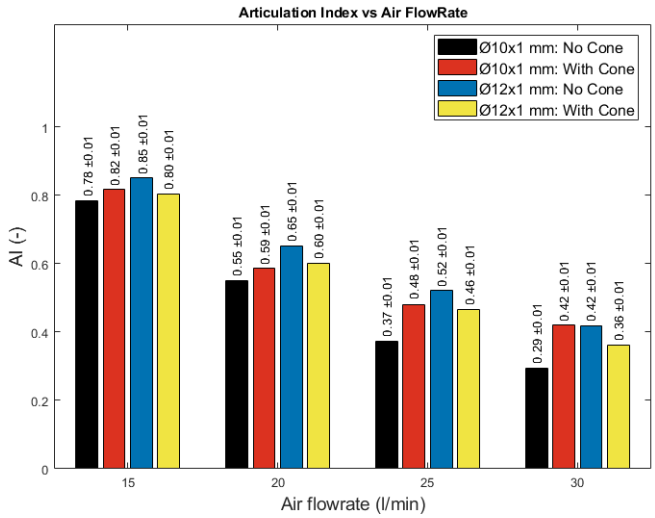

Figure A.8: AI comparison: No Cone vs With Cone for different tube diameters.

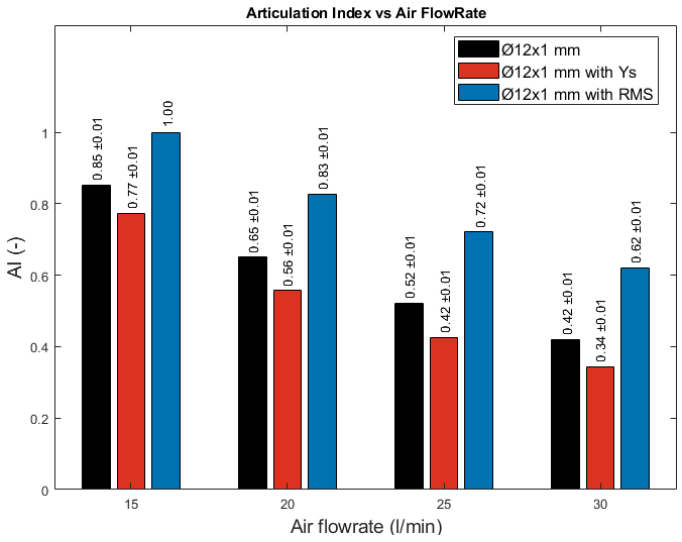

Figure A.9: AI comparison for different splitter designs.

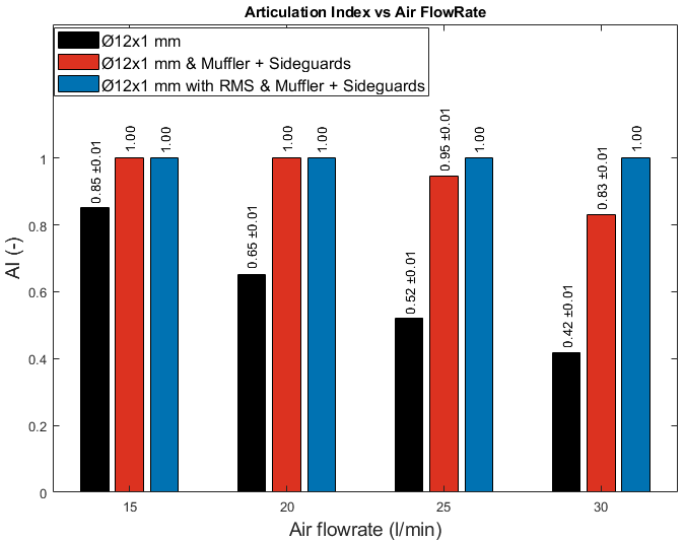

Figure A.10: AI comparison of RMS with add-ons.

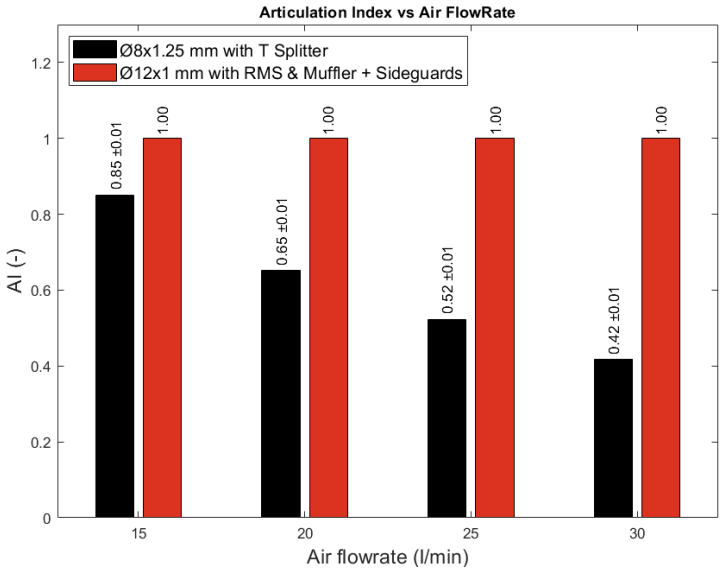

Figure A.11: AI comparison: first and last PPE iteration

APPENDIX B

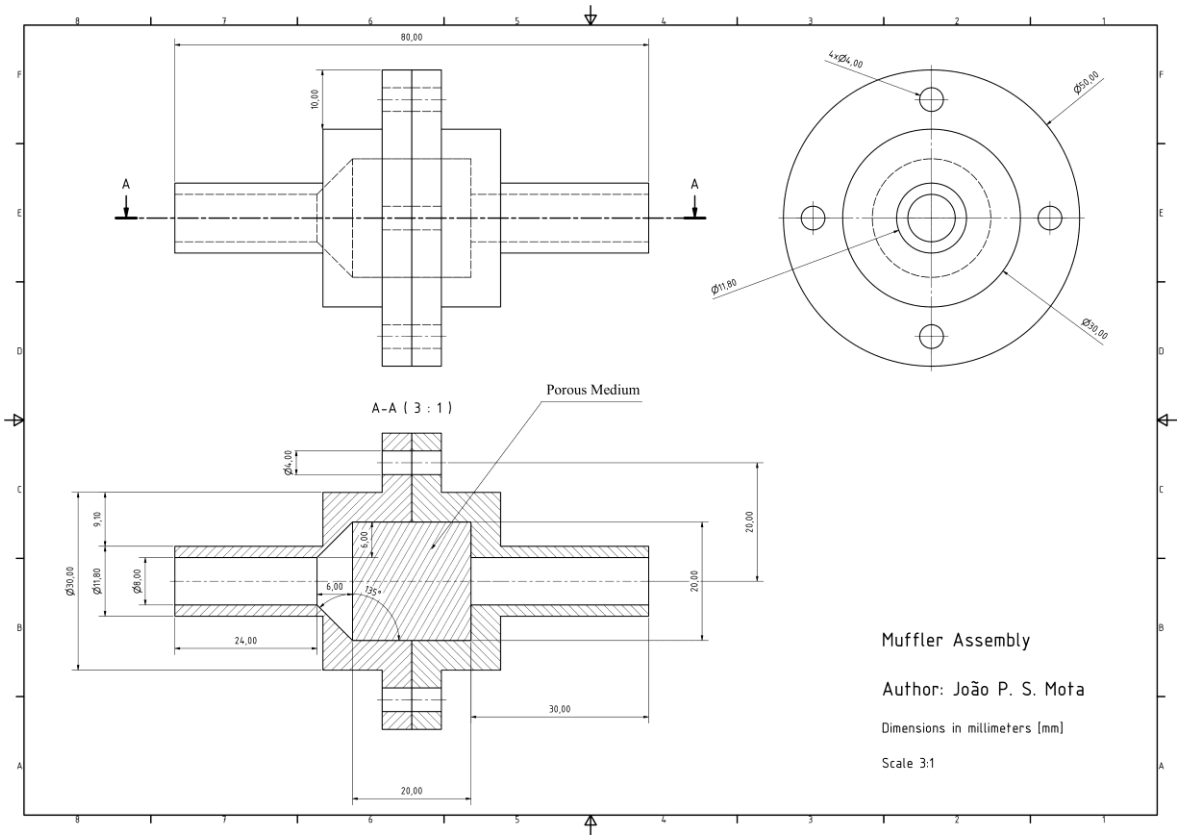

Figure B.1: Technical Drawing of the Muffler Assembly.

APPENDIX C

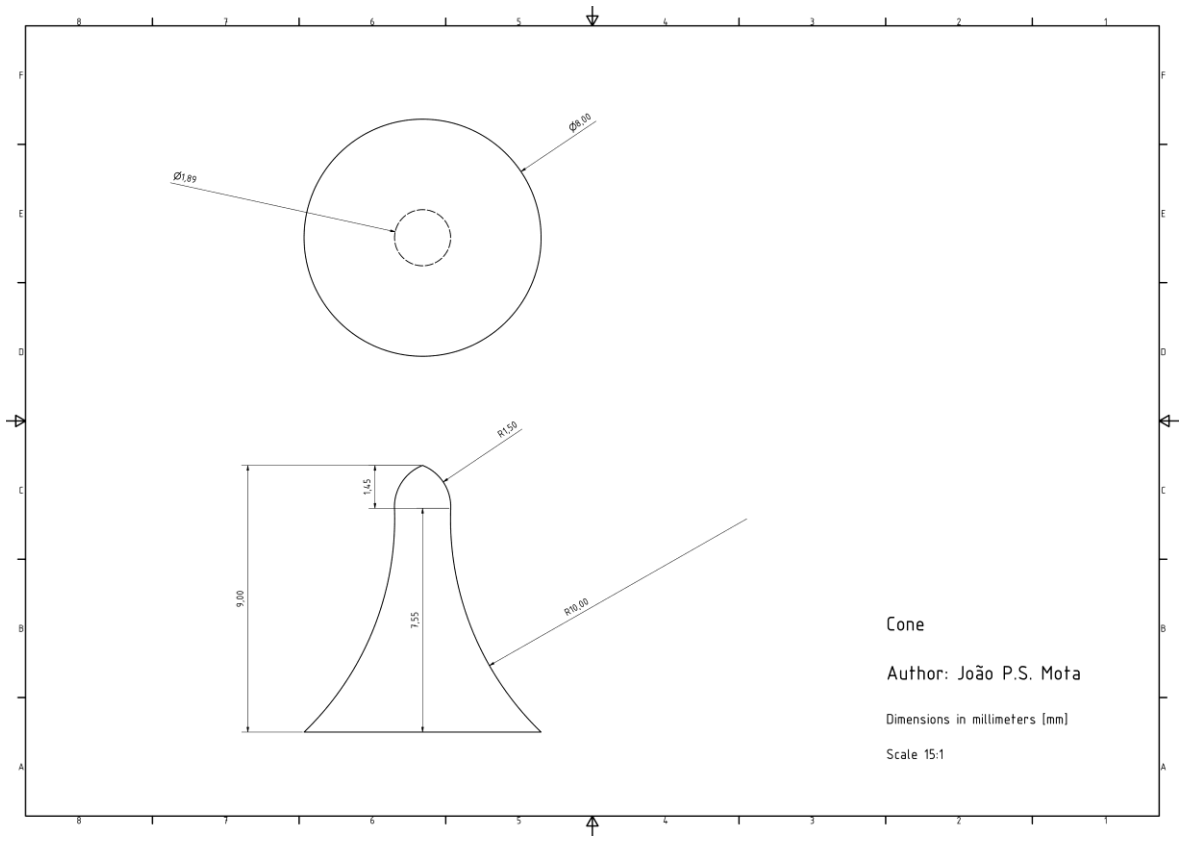

Figure C.1: Technical Drawing of the Plenum Cone.

APPENDIX D

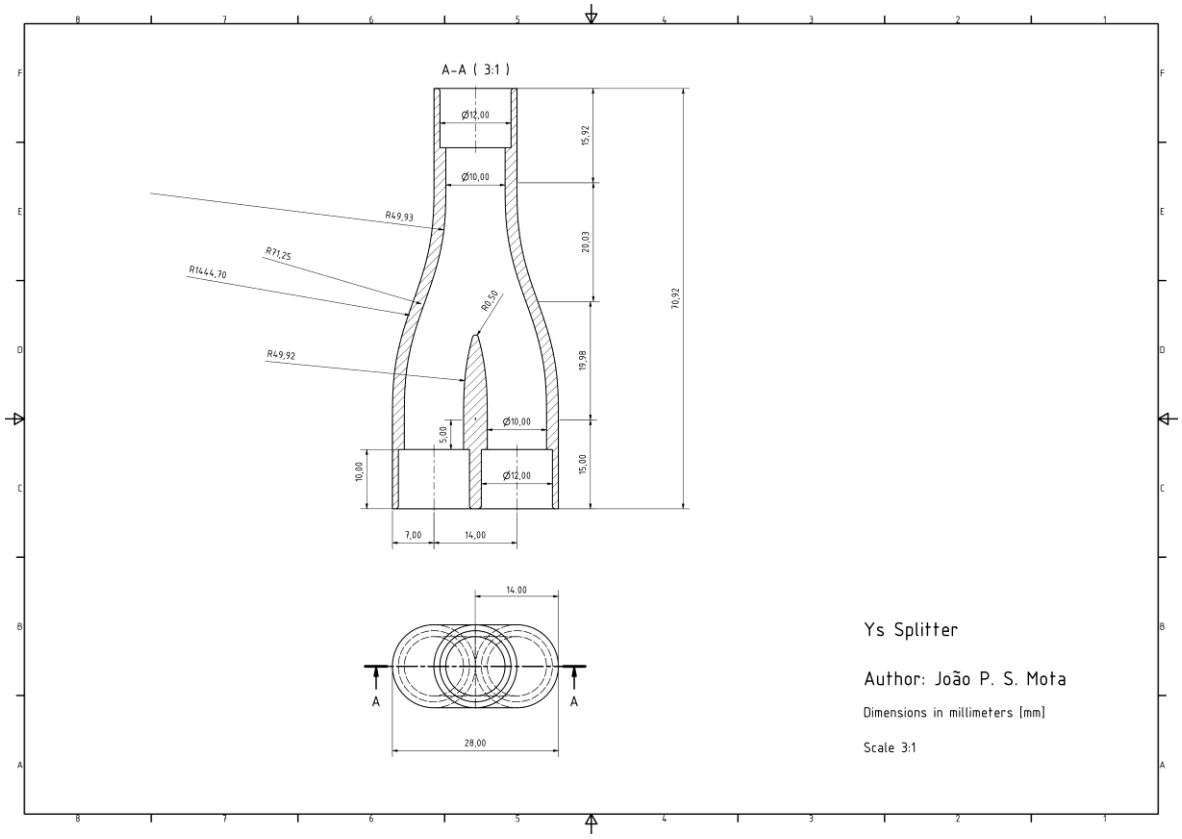

Figure D.1: Technical Drawing of the Ys Splitter.

APPENDIX E

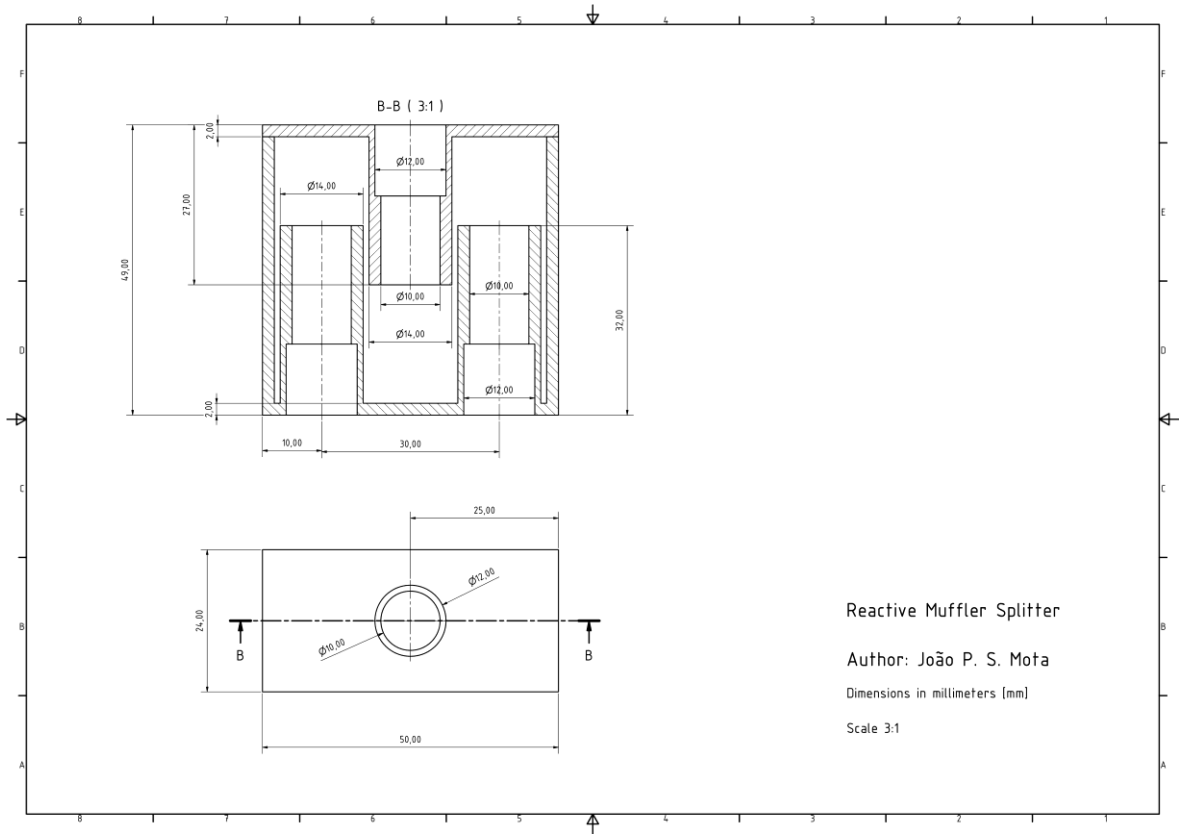

Figure E.1: Technical Drawing of the Reactive Muffler Splitter (RMS).